Open access • Journal Article • DOI:10.1137/070684392

Error Estimation for Reduced-Order Models of Dynamical Systems — Source link

Chris Homescu, Linda R. Petzold, Radu Serban

Published on: 01 Apr 2007 - Siam Review (Society for Industrial and Applied Mathematics)

Topics: Dynamical systems theory

UCRL-TR-201494

Error Estimation for Reduced Order Models of Dynamical Systems

C. Homescu, L.R. Petzold, and R. Serban

December 16, 2003

DISCLAIMER

This research was supported under the auspices of the U.S. Department of Energy by the University of California, Lawrence Livermore National Laboratory under contract No. W-7405-Eng-48.

Error Estimation for Reduced Order Models of Dynamical Systems *

Chris Homescu † Linda R. Petzold ‡ Radu Serban §

Abstract

The use of reduced order models to describe a dynamical system is pervasive in science and engineering. Often these models are used without an estimate of their error or range of validity. In this paper we consider dynamical systems and reduced models built using proper orthogonal decomposition. We show how to compute estimates and bounds for these errors, by a combination of the small sample statistical condition estimation method and of error estimation using the adjoint method.

More importantly, the proposed approach allows the assesment of so-called *regions of validity* for reduced models, i.e., ranges of perturbations in the original system over which the reduced model is still appropriate. This question is particularly important for applications in which reduced models are used not just to approximate the solution to the system that provided the data used in constructing the reduced model, but rather to approximate the solution of systems perturbed from the original one.

Numerical examples validate our approach: the error norm estimates approximate well the forward error while the derived bounds are within an order of magnitude.

*This work was supported by DOE DE-FG03-00ER25430, NSF/NCSA ACI-9619019, and NSF/ITR ACI-0086061. The work of the last author was performed under the auspices of the U.S. Department of Energy by the University of California, Lawrence Livermore National Laboratory under contract No. W-7405-Eng-48.

†Department of Computer Science, University of California, Santa Barbara, California 93106 (homescu@cs.ucsb.edu)

‡Department of Computer Science, University of California, Santa Barbara, California 93106 (petzold@engineering.ucsb.edu)

§Center for Applied Scientific Computing, Lawrence Livermore National Laboratory, Livermore, California 94551 (radu@llnl.gov)

Notation

y	Solution of the original ODE system
$f(t, y, p)$	Right hand side function for the original ODE
$\mathbf{J}(y, t, p)$	Jacobian of f with respect to y
$\mathbf{K}(y, t, p)$	Partial derivative of f with respect to the model parameters p
Φ_y	Fundamental matrix evaluated along the trajectory y
Y	Solution of a perturbed ODE system
δy_0	Perturbation in the initial conditions
δp	Perturbation in the model parameters
$\bar{y}$	Mean value of POD data
y^S	Solution of the reduced model in subspace coordinates
$\hat{y}$	Solution of the reduced model in full coordinates
S	POD affine subspace
ρ	Projection matrix onto S; $\rho \in \mathbb{R}^{n \times k}$
P	Projection matrix expressed in full coordinates; $P = \rho\rho^T \in \mathbb{R}^{n \times n}$
e	Error vector for the original ODE; $e = \hat{y} - y$
e_0, e_i	Components of e; $e_i \in S$, $e_0 \in S^\perp$
E_1	Error vector for the perturbed ODE; $E_1 = \hat{Y} - Y$
E_2	Cummulative error vector for the perturbed ODE; $E_2 = \hat{Y} - y$
Δ	Additional error due to perturbation; $\Delta = E_1 - e$
Δ_0, Δ_i	Components of Δ; $\Delta_i \in S$, $\Delta_0 \in S^\perp$
λ_y	Solution of an n-dimensional adjoint system evaluated along the trajectory y
μ_y	Solution of a k-dimensional adjoint system evaluated along the trajectory y
Ψ	Sensitivity matrix
z	Unit vector uniformly and randomly selected from a unit sphere
W_n	Wallis factor of order n

1 Introduction

Model reduction of dynamical systems described by differential equations is pervasive in science and engineering [1]. Reduced models are used for efficient simulation [13, 26] and control [24, 14]. Moreover, the process of creating low-order models forces the researcher to isolate and quantify the dominant physical mechanisms, revealing effective design decisions that would not have been identified through numerical simulation, experimentation or "black box" optimization methods [25].

The Proper Orthogonal Decomposition (POD) method has been used extensively in a variety of fields including fluid dynamics [19], identification of coherent structures [10, 17], control [18, 23] and inverse problems [15]. This method proved to be equally effective for industrial applications in many fields, such as damage detection in structures [3], supersonic jet modelling [5], turbine flows [6], thermal processing of foods [2], and study of the dynamic wind pressures acting on buildings [12], to name only a few. A detailed description of the POD approach as a reduction method is presented in [10], where it is shown that, for a given number of modes n, POD is the most efficient among all linear decompositions as it retains, on average, the greatest possible kinetic energy . In other words, POD provides the most efficient way of capturing the dominant components of an infinite-dimensional process with only finitely many, and often surprisingly few, modes.

But as soon as one contemplates the use of a reduced model (such as POD-based reduced models), questions concerning the quality of the approximation become paramount. To judge the quality of the reduced model, it is especially important to analyze the error of this model, i.e., the difference between the approximate and the exact solution. An algorithm for computing the error of a class of reduction methods based on projection techniques is presented in [27]. In this approach, the original problem is linearized around the initial time, and therefore the resulting first-order error estimates are valid for only a small number of time steps (during which the Jacobian matrix can be considered constant). In the context of fluid dynamics, bounds for the errors resulting from POD model reduction were computed in [15], with results applied to the Navier Stokes equations in 2-D. In this work, the approximation error was decomposed into a contribution that arises due to the POD approximation in space (contribution measured in terms of the spectral properties specifying the POD basis) and the usual approximation error due to backwards Euler scheme for time integration. However, the resulting estimates make use of certain inequalities that, although valid for the nonlinear evolution problem considered, may not be satisfied for other examples. Error estimates for the reduced models by the adjoint approach were derived in [20]. In this work, the authors employ the dual-weighted-residual (DWR) method, which uses the solution of an adjoint system to obtain an estimate of the error for a certain functional of the solution.

First-order estimates of the POD errors have also been used as tools for deciding which regions of the domain require more information than that available from the reduced model only [16]. Given an approximate solution (with unknown accuracy) of the reduced model, an augmented POD basis is constructed and the first order change in the solution due to the addidtional basis functions is computed. By comparing against the results from a solution of known accuracy, such as one of the snapshots used to generate the POD basis, the authors are able to decide on the need for domain decomposition as well as its spatial extent.

In the present work, we take the analysis of reduced models one step further by studying and quantifying the influence of perturbations in the original system on the quality of the approximation given by the reduced model. This question is of particular interest in applications (such as control and inverse problems) in which reduced models are used not just to approximate the solution of original system that provided the data used in constructing the reduced model, but rather to approximate the solution of systems perturbed from the original one. To the best of our knowledge, there are no published results to address the model reduction error of such perturbed systems.

As described in details over the next sections, we base our approach on a combination of the small sample statistical condition estimation (SCE) method [11] and adjoint models. Under this framework, we are able to define so-called *regions of validity of the reduced models*, that is, ranges of

perturbations in the original system over which the reduced model is still appropriate. We consider perturbations in both the initial conditions and in parameters describing the dynamical system itself. The proposed approach is particularly attractive as the resulting error bounds do not rely in the solution of the perturbed system. In this sense, we provide an *a-priori* assesment of the validity of the model-reduction approximation.

Unlike the method presented in [27], our estimates and bounds are valid over the entire time interval considered and not only in a neighborhood of the initial time. Moreover, we obtain esimates for the continuous error, as opposed to its discrete computation. Although we study only a particular projection-based model reduction technique (POD) among those considered in [27], the methodology developed here for POD can be easily extended to other types of projection. Compared to the approach taken in [15], our method is applicable to a larger class of problems, our main requirement being that the norm of the POD-based error is small enough for the linearized error equation to be a good enough approximation. Furthermore, our estimates are independent of the time integration method. Finally, we note that our use of adjoint models for error estimation is similar to that employed in [20]. However, as will be seen below, the use of the SCE method enables the derivation of error "condition numbers" and allows effective treatment of the regions of validity problem.

The remainder of this paper is organized as follows. In §2.1 and §2.2 we briefly describe the use of POD for model reduction and the SCE method for norm estimation, respectively. In §2.3 we motivate our proposed approach of using SCE, combined with error estimation using the adjoint method, to estimate the errors due to the use of a reduced order model. In §3 we analyze errors arising purely from the model reduction itself. We consider both the total approximation error and the subspace integration error. In §4 we analyze regions of validity of POD reduced models. §5 presents numerical results for several example problems, including semi-discretizations of time-dependent PDEs, chemical reaction mechanisms, and plant physiology. Finally, §6 summarizes our conclusions and indicates directions of future research.

2 Background

2.1 POD-based reduced models

POD provides a method for finding the best approximating affine subspace to a given set of data. When using POD for model reduction of dynamical systems, the data are time snapshots of the solution obtained via numerical simulations or from experiments.

Consider the ODE system

$$\frac{dy}{dt} = f(y,t)\,, \quad y(t_0) = y_0\,, \tag{1}$$

for $t \in [t_0, t_f]$, with $y, y_0 \in \mathbb{R}^n$ and $f : \mathbb{R}^n \times \mathbb{R} \to \mathbb{R}^n$. Consider next the solutions of (1) at m time points, collected in the $n \times m$ matrix $\mathcal{Y} = [y(t_1) - \bar{y}, y(t_2) - \bar{y}, \ldots y(t_m) - \bar{y}]$, where $\bar{y}$ is the mean of these observations. POD seeks a subspace $S \in \mathbb{R}^n$ and the corresponding projection matrix P_S so that the total square distance

$$\|\mathcal{Y} - P\mathcal{Y}\|^2 = \sum_{i=1}^{m} \| \left(y(t_i) - \bar{y}\right) - P\left(y(t_i) - \bar{y}\right) \|^2$$

is minimized. Let $\lambda_1 \geq \lambda_2 \geq \cdots \geq \lambda_m \geq 0$ be the ordered eigenvalues of the *correlation matrix* $R = \mathcal{Y}\mathcal{Y}^T$. Then the minimum value of $\|\mathcal{Y} - P\mathcal{Y}\|^2$ over all k-dimensional subspaces S, with $k \leq n$, is given by $\sum_{j=k+1}^{n} \lambda_j$. Moreover, the minimizing S is the invariant subspace corresponding to the eigenvalues $\lambda_1, \ldots, \lambda_k$. Using the singular value decomposition [7] of the observation matrix, $U^T \mathcal{Y} V = \Sigma$, the projection matrix corresponding to the optimal POD subspace S is obtained as

$$P = \rho\rho^T \in \mathbb{R}^{n \times n}\,, \tag{2}$$

where ρ is the matrix of projection onto S, the subspace spanned by the reduced basis obtained from the SVD. The matrix $\rho \in \mathbb{R}^{n\times k}$ consists of the columns V_i $(i = 1 \dots k)$, the singular vectors corresponding to the k largest singular values.

In a coordinate system embedded in S, the projection of a point y onto S is represented by $y^S = \rho^T(y - \bar{y}) \in \mathbb{R}^k$, while in the full space, the same projection is expressed as $\tilde{y} = P(y-\bar{y})+\bar{y} \equiv \rho y^S + \bar{y} \in \mathbb{R}^n$.

A POD-based reduced model that approximates the original problem (1) can then be constructed [22] by projecting onto S the vector field $f(s,t)$ at each point $s \in S$. If y^S are the subspace coordinates of s, then

$$\frac{dy^S}{dt} = \rho^T f(\rho y^S + \bar{y}, t)\,, \quad y^S(t_0) = \rho^T(y_0 - \bar{y})\,. \tag{3}$$

From the above, it is easy to see that the approximate solution $\hat{y}$ is the solution of the ODE IVP:

$$\frac{d\hat{y}}{dt} = Pf(\hat{y}, t)\,, \quad \hat{y}(t_0) = P(y_0 - \bar{y}) + \bar{y}\,. \tag{4}$$

2.2 Small sample statistical method for condition estimation

The small sample statistical condition estimation (SCE) method, originally proposed in [11], offers an efficient means for condition estimation for general matrix functions, at the cost of allowing moderate relative errors in the estimate. The basic idea is described below (for complete details, see [11, 8]).

For any vector $v \in \mathbb{R}^n$, if z is selected uniformly and randomly from the unit sphere $\mathbb{S}_{n-1}$, the expected value of $z^T v$ is proportional to the norm of v:

$$E(|z^T v|) = W_n ||v||$$

The proportionality factor, called the *Wallis factor*, depends only on n. It is defined as $W_1 = 1$ and

$$W_n = \begin{cases} \dfrac{1\cdot 3\cdots(n-2)}{2\cdot 4\cdots(n-1)} & \text{for } n \text{ odd} \\ \dfrac{2}{\pi}\dfrac{2\cdot 4\cdots(n-1)}{1\cdot 3\cdots(n-2)} & \text{for } n \text{ even} \end{cases}$$

and can be approximated by $W_n \approx \sqrt{\dfrac{2}{\pi(n-\frac{1}{2})}}$.

Thus, we use the expression $\xi = \dfrac{|z^T v|}{W_n}$ to estimate the norm $||v||$. This estimate is first order in the sense that the probability of a relative error in the estimate is inversely proportional to the size of the error. That is, for $\gamma > 1$, we have

$$\Pr\left(\frac{||v||}{\gamma} \le \xi \le \gamma||v||\right) \ge 1 - \frac{2}{\pi\gamma} + O\left(\frac{1}{\gamma^2}\right)\,.$$

Additional function evaluations can improve the estimation procedure.

Suppose that we obtain estimates $\xi_1, \xi_2, \dots, \xi_p$ corresponding to orthogonal vectors $z_1, z_2, \dots, z_q$ selected uniformly and randomly from the unit sphere $\mathbb{S}_{n-1}$. The expected value of the norm of the projection of v onto the span $\mathcal{Z}$ generated by $z_1, z_2, \dots, z_q$ is

$$E\left(\sqrt{|z_1^T v|^2 + |z_2^T v|^2 + \cdots + |z_q^T v|^2}\right) = \frac{W_n}{W_q}||v||\,.$$

Table 1: Comparison of two methods for estimation of vector norms withs SCE. Method A uses $z \in \mathbb{S}_{n-1}$. Method B uses $z \in \mathbb{S}_{n'-1}$.

w	$\Pr(\|v\|/\gamma \le \nu(k) \le \gamma\|v\|)$					
	$q=1$		$q=2$		$q=3$	
	A	B	A	B	A	B
2	0.5613	0.5800	0.7790	0.8431	0.8747	0.9168
3	0.7757	0.8030	0.9186	0.9324	0.9648	0.9740
5	0.8851	0.8929	0.9711	0.9751	0.9920	0.9942
10	0.9422	0.9472	0.9930	0.9935	0.9990	0.9993
100	0.9942	0.9946	0.9999	0.9999	1.0000	1.0000
1000	0.9994	0.9995	1.0000	1.0000	1.0000	1.0000

The estimate $\nu(p) = \dfrac{W_q}{W_n}\sqrt{|z_1^T v|^2 + |z_2^T v|^2 + \cdots + |z_q^T v|^2}$ has q^{th} order accuracy, i.e., a relative error of size γ in the estimate occurs with probability proportional to γ^{-q}:

$$\Pr\left(\frac{||v||}{\gamma} \le \nu(q) \le \gamma||v||\right) \ge 1 - \frac{1}{p!}\left(\frac{2}{\pi\gamma}\right)^q + O\left(\frac{1}{\gamma^{q+1}}\right).$$

Usually at most four random vectors are required in practice. The corresponding probabilities satisfy [11]:

$$\Pr\left(\frac{||v||}{\gamma} \le \nu(2) \le \gamma||v||\right) \approx 1 - \frac{\pi}{4\gamma^2},$$
$$\Pr\left(\frac{||v||}{\gamma} \le \nu(3) \le \gamma||v||\right) \approx 1 - \frac{32}{3\pi^2\gamma^3},$$
$$\Pr\left(\frac{||v||}{\gamma} \le \nu(4) \le \gamma||v||\right) \approx 1 - \frac{81\pi^2}{512\gamma^4}.$$

NOTE. We conclude this section with an observation that will help improve the efficiency of some subsequent computations. Consider estimating the norm of an n-dimensional vector $v \in \mathbb{R}^n$ using SCE. This can be achieved by evaluating scalar products of the form $z^T v$, with z randomly and uniformly selected from the sphere $\mathbb{S}_{n-1}$. However, if it is known that $v \in M$, with M an n'-dimensional subspace of $\mathbb{R}^n$, a more accurate estimate is obtained if we select vectors from the unit sphere $\mathbb{S}_{n'-1}$ in M and use their representation z' in $\mathbb{R}^n$. The data in Table 1 shows the probability that the vector norm estimate lies within a factor $\gamma \in \{2, 3, 5, 10, 100, 1000\}$ of the true norm $\|v\|$. Method A uses $z \in \mathbb{S}_{n-1}$, while method B uses $z \in \mathbb{S}_{n'-1}$. For this numerical example we have used $n = 1000$ and $n' = 10$. Results are given for $q = 1, 2, 3$, where q is the number of unit vectors used in the SCE estimate (5). The probabilities in Table 1 were computed from $100,000$ tests each.

2.3 SCE for estimation of approximation errors in model reduction

All error estimates derived in this paper start from linearizations of one of the ODEs (1), (3), (4), or perturbations of these. As a consequence, the error estimates are based on solutions of linear error equations. To estimate the norm $\|e(t_f)\|$ of an error vector $e(t) \in \mathbb{R}^n$ at $t = t_f$, we need to evaluate quantities $z_j^T e(t_f)$ for some random vector z_j selected uniformly from the unit sphere $\mathbb{S}_{n-1}$. An estimate of the norm of the error can be obtained as

$$||e(t_f)|| \approx \frac{W_q}{W_n}\sqrt{\sum_{j=1}^{q} |z_j^T e(t_f)|^2}. \tag{5}$$

The scalar products $z_j^T e(t_f)$ can be computed efficiently using an adjoint model (to the corresponding linear error equation) with final conditions at t_f based on the vector z_j.

However, this approach naturally raises the question: "What is the advantage of using (typically more than one) solution of adjoint systems to estimate the norm of a quantity that can be otherwise obtained with only one forward ODE solution (of the error equation)?" Our proposed approach is motivated by the fact that we are interested not only in finding the errors for one given ODE system, but rather in estimating (as efficiently as possible) the behavior of such errors for *families of related ODE systems*. In Section 4 we are concerned with evaluating *regions of validity of reduced models* or, in other words, evaluating the range of perturbations in the original ODE (1) over which the reduced model (3) is still appropriate. An approach based on forward error equations involves repeated solutions of such error equations (for each value of interest of the perturbation). On the other hand, an approach combining SCE estimates and adjoint models (as described in the next sections) can be used to define what we term "condition numbers" for these error equations. While these condition numbers can provide only approximate upper bounds for the norms of the errors under investigation, they have the undeniable advantage of allowing *a-priori* estimates of the errors induced by perturbations, i.e., before having to solve such a perturbed system (or even a reduced perturbed system).

In the context of ODE integration, the SCE method, combined with adjoint models, has been used in [4] for estimation and control of the global integration error.

3 Estimation of the approximation error

We begin by obtaining estimates for the difference between the solution of the POD-reduced model (4) and the solution for the original equation (1). Let $\tilde{y}(t)$ be the projection onto S of the solution $y(t)$. Then the total approximation error $e(t) = \hat{y}(t) - y(t)$ can be split into the subspace approximation error $e_\perp(t) = \tilde{y}(t) - y(t)$ and the error introduced by the integration in the subspace S, $e_i(t) = \hat{y}(t) - \tilde{y}(t)$:

$$e(t) = \hat{y}(t) - y(t) = (\hat{y}(t) - \tilde{y}(t)) + (\tilde{y}(t) - y(t)) = e_i(t) + e_\perp(t) \ . \tag{6}$$

The error component $e_\perp$ is orthogonal to S, while the component e_i is parallel to S (see Fig. 1). Algebraically, this is expressed as $Pe_\perp(t) = 0$ and $Pe_i(t) = e_i(t)$.

3.1 Total approximation error

First we derive an estimate for the total error e. Subtracting (1) from (4), the error function satisfies

$$\frac{de}{dt} = Pf(\hat{y},t) - f(y,t) = Pf(\hat{y},t) - f(\hat{y},t) + f(\hat{y},t) - f(y,t) = (P-I)f(\hat{y},t) - \mathbf{J}(\hat{y},t)(y-\hat{y}) + O(||e||^2) \ ,$$

where $\mathbf{J}$ is the Jacobian of the function f, i.e., $\mathbf{J} = \partial f / \partial y$. Thus, to a first order approximation, the error function satisfies

$$\frac{de}{dt} = \mathbf{J}(\hat{y},t)e(t) - (I-P)f(\hat{y},t) \ , \quad e(t_0) = -(I-P)(y_0 - \bar{y}) \ . \tag{7}$$

Let the matrix function $\Phi_{\hat{y}}(t) \in \mathbb{R}^{n \times n}$ satisfy

$$\frac{d\Phi_{\hat{y}}}{dt} = \mathbf{J}(\hat{y},t)\Phi_{\hat{y}} \ , \quad \Phi_{\hat{y}}(t_0) = I_n \ , \tag{8}$$

where the subscript $\hat{y}$ for $\Phi_{\hat{y}}$ indicates that the Jacobian is evaluated at $\hat{y}$. Then

$$e(t_f) = -\int_{t_0}^{t_f} \Phi_{\hat{y}}(t_f)\Phi_{\hat{y}}^{-1}(s)(I-P)f(\hat{y}(s),s)\,ds - \Phi_{\hat{y}}(t_f)(I-P)(y_0 - \bar{y}) \ .$$

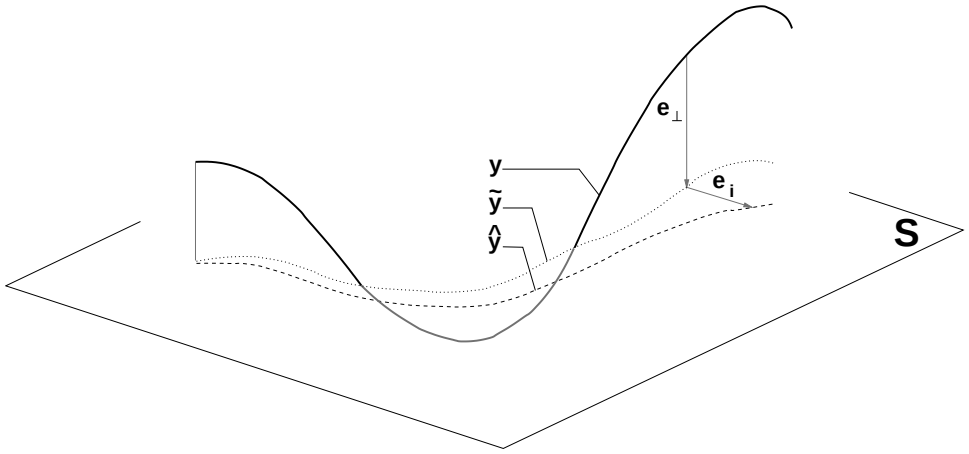

Figure 1: Solution and error components for POD-reduced models. y is the solution of the original ODE, $\tilde{y}$ is its projection on the affine subspace S, and $\hat{y}$ is the solution of the reduced model. The error component $e_\perp$ lies in $S^\perp$, while the subspace integration error component lies in S.

For a random vector z uniformly selected from the unit sphere $\mathbb{S}_{n-1}$ we have:

$$z^T e(t_f) = -\int_{t_0}^{t_f} z^T \Phi_{\hat{y}}(t_f)\Phi_{\hat{y}}^{-1}(s)(I-P)f(\hat{y}(s),s)\,ds - z^T\Phi_{\hat{y}}(t_f)(I-P)(y_0-\bar{y})\ .$$

It is straightforward to verify that the solution $\lambda_{\hat{y}} \in \mathbb{R}^n$ of the adjoint system

$$\frac{d\lambda_{\hat{y}}}{dt} = -\mathbf{J}^T(\hat{y},t)\lambda_{\hat{y}}\,, \quad \lambda_{\hat{y}}(t_f) = z \tag{9}$$

satisfies

$$\begin{aligned}\lambda_{\hat{y}}^T(s) &= z^T\Phi(t_f)\Phi^{-1}(s)\\ \lambda_{\hat{y}}^T(t_0) &= z^T\Phi(t_f)\ .\end{aligned}$$

As before, the subscript $\hat{y}$ indicates that the Jacobian in the adjoint system (9) is evaluated at $\hat{y}$. Therefore, the quantity $z^T e(t_f)$ is simply

$$z^T e(t_f) = -\int_{t_0}^{t_f} \lambda_{\hat{y}}^T(s)(I-P)f(\hat{y}(s),s)\,ds - \lambda_{\hat{y}}^T(t_0)(I-P)(y_0-\bar{y})\,,$$

and the SCE estimate for the norm of $e(t_f)$ is given by

$$||e(t_f)|| \approx \frac{W_q}{W_n}\left[\sum_{j=1}^{q}|z_j^T e(t_f)|^2\right]^{1/2} =$$

$$\frac{W_q}{W_n}\left[\sum_{j=1}^{q}\left|\int_{t_0}^{t_f}\lambda_{\hat{y}}^T(s)(I-P)f(\hat{y}(s),s)\,ds + \lambda_{\hat{y}}^T(t_0)^T(I-P)(y_0-\bar{y})\right|^2\right]^{1/2}. \tag{10}$$

The integral in the above equation can be evaluated during the solution of (9) by appending the quadrature equation

$$\frac{d\psi}{dt} = -\lambda_{\hat{y}}^T(t)(I-P)f(\hat{y}(t),t)\,, \quad \psi(t_f) = 0\,, \tag{11}$$

so that the value of the integral is $\psi(t_0)$.

Algorithm 1 summarizes the computation of an SCE estimate of the norm of the total error.

Algorithm 1 Estimate for the total approximation error

provide the matrix of measurement data $\mathcal{Y}$
set the POD dimension k
compute mean value of data $\bar{y}$ and construct POD projection matrices ρ and P
construct q orthogonal vectors selected uniformly and randomly from the unit sphere $\mathbb{S}_{n-1}$
solve (3) for y^S
$\hat{y}(t) = \rho y^S(t) + \bar{y}$
initialize $s = 0$
for $i = 1$ to q **do**
  set $\lambda_{\hat{y}}(t_f) \leftarrow z_i$
  solve (9)+(11) for $\lambda_{\hat{y}}$ and ψ
  update $s \leftarrow s + \left[\psi(t_0) + \lambda_{\hat{y}}^T(t_0)^T(I-P)(y_0 - \bar{y})\right]^2$
end for
compute Wallis factors W_q and W_n
compute the SCE norm estimate $e = (W_q/W_n) \times \sqrt{s}$

NOTE. One may be tempted to try to compute the SCE norm estimate more efficiently by using a POD-reduced adjoint system to evaluate $\lambda_{\hat{y}}$ in (10). Although the same projection can be used to model-reduce the adjoint system, this approach still requires knowledge of the mean of the adjoint solution which is unavailable without a solution of the adjoint system (9). In other words, the approximation subspace S^λ is parallel to S but not identical to it.

This issue can be circumvented if we are not considering error components outside the subspace S. This approach is presented next.

3.2 Subspace integration error

We start from the definition of the total POD approximation error of (6). Differentiating $e_\perp(t) + e_i(t) = \hat{y}(t) - y(t)$ and substituting the ODEs for y and $\hat{y}$, we get

$$\frac{de_\perp}{dt} + \frac{de_i}{dt} = Pf(\hat{y},t) - f(y,t)\ .$$

Projecting the above equation onto S (by multiplying on the left by P) and taking advantage of the fact that $Pe_\perp = 0$, yields the following IVP for the subspace integration error:

$$\frac{de_i}{dt} = P\left(f(\hat{y},t) - f(y,t)\right)\ , \quad e_i(t_0) = 0\,, \tag{12}$$

where we have used that $P^2 = P$. The initial condition is due to the fact that the starting point $\hat{y}(t_0)$ is the projection $\tilde{y}(t_0)$ of $y(t_0)$ onto S. Thus the subspace integration error is governed by an ODE with the subspace approximation error $e_\perp(t)$ as forcing term. Linearizing around the trajectory $\hat{y}(t)$ gives the following approximation to (12):

$$\frac{de_i}{dt} = P\mathbf{J}(\hat{y},t)e_i + P\mathbf{J}(\hat{y},t)e_\perp\,, \quad e_i(t_0) = 0\,. \tag{13}$$

In the S coordinate system defined by the coordinate transformation:

$$e_i^S = \rho^T e_i \in \mathbb{R}^k$$
$$e_i \equiv \hat{e}_i = \rho e_i^S\ ,$$

the above equation can be written as

$$\frac{de_i^S}{dt} = \rho^T P\mathbf{J}(\hat{y},t)\left(\rho e_i^S + e_\perp\right) = \rho^T\mathbf{J}(\hat{y},t)\rho e_i^S + \rho^T\mathbf{J}(\hat{y},t)e_\perp\ ,$$

where the identity $\rho^T\rho = I_k$ was used. Therefore, e_i^S satisfies

$$\frac{de_i^S}{dt} = \rho^T \mathbf{J}(\hat{y},t)\rho e_i^S + \rho^T \mathbf{J}(\hat{y},t)e_\perp\,, \quad e_i^S(t_0) = 0\,. \tag{14}$$

If $\phi_{\hat{y}} \in \mathbb{R}^{k\times k}$ is the fundamental matrix, solution of

$$\frac{d\phi_{\hat{y}}}{dt} = \rho^T \mathbf{J}(\hat{y},t)\rho\phi_{\hat{y}}\,, \quad \phi_{\hat{y}}(t_0) = I_k\,,$$

then, for a random vector z^S uniformly selected from the unit sphere $\mathbb{S}_{k-1}$, we have

$$(z^S)^T e_i^S(t_f) = \int_{t_0}^{t_f} (z^S)^T \phi_{\hat{y}}(t_f)\phi_{\hat{y}}^{-1}(s)\rho^T \mathbf{J}(\hat{y}(s),s)e_\perp(s)\,ds\ .$$

Consider next the adjoint system

$$\frac{d\mu_{\hat{y}}}{dt} = -\rho^T \mathbf{J}^T(\hat{y},t)\rho\mu_{\hat{y}}\,, \quad \mu_{\hat{y}}(t_f) = z^S\,, \tag{15}$$

the solution of which satisfies $\mu_{\hat{y}}^T(s) = (z^S)^T\phi_{\hat{y}}(t_f)\phi_{\hat{y}}^{-1}(s)$. Then,

$$(z^S)^T e_i^S(t_f) = \int_{t_0}^{t_f} \mu_{\hat{y}}^T(s)\rho^T \mathbf{J}(\hat{y}(s),s)e_\perp(s)\,ds\ .$$

The SCE approximation for the norm of the subspace integration error at the final time is

$$||e_i(t_f)|| \approx \frac{W_q}{W_n}\sqrt{\sum_{j=1}^{q} |(z_j^S)^T e_i^S(t_f)|^2} = \frac{W_q}{W_n}\sqrt{\sum_{j=1}^{q} \left|\int_{t_0}^{t_f} \mu_{\hat{y}}^T(s)\rho^T \mathbf{J}(\hat{y}(s),s)e_\perp(s)\,ds\right|^2}\ . \tag{16}$$

Although the SCE approach only provides an approximation of the subspace integration error (moreover, at the cost of additional backward integration of adjoint systems) and is therefore not a useful alternative to integrating the forward error equation (12), it appears here only as an intermediate step towards obtaining a bound on this error. Indeed, let

$$\theta^j(s) = \mathbf{J}^T(\hat{y}(s),s)\rho_k\mu_{\hat{y}}(s)\,, \quad \theta^j(s) \in \mathbb{R}^{N_y} \quad \text{and } w_j = \int_{t_0}^{t_f} (\theta^j)^T(s)e_\perp(s)\,ds\,,$$

where j denotes correspondence to some unit vector z_j^S in (15). Then

$$|w_j| \le \int_{t_0}^{t_f} |(\theta^j)^T(s)e_\perp(s)|\,ds \le \left(\int_{t_0}^{t_f}\sum_{i=1}^{N_y}|\theta_i^j(s)|\,ds\right)||e_\perp||_{L_\infty}\,. \tag{17}$$

Therefore, defining $\kappa_j(e_i) \triangleq ||\theta^j||_{L_1} = \int_{t_0}^{t_f}\sum_{i=1}^{N_y}|\theta_i^j(s)|\,ds$, we have

$$||e_i(t_f)|| \le \kappa(e_i)\cdot||e_\perp||_{L_\infty}\,, \tag{18}$$

where

$$\kappa(e_i) = \frac{W_q}{W_n}\sqrt{\sum_{j=1}^{q}\kappa_j^2(e_i)}$$

can be interpreted as a "condition number" for the subspace integration error.

The expressions derived above require knwledge of the projection error $e_\perp$ at all times in $[t_0, t_f]$ (for the integration of the forward error equation (12) or for the quadrature in (16)) or of its L_∞ norm, $||e_\perp||_{L_\infty}$, in (18). While the expression of the projection error may not be readily available, its norm can be easily related to the error associated with the choice of the POD subspace. For this, a more convenient definition of the POD approximation is to find a subspace $S \in \mathbb{R}^n$ which minimizes the total square distance d^2 defined as

$$d^2 = \| (y - \bar{y}) - P (y - \bar{y}) \|_{L_2}^2 = \int_{t_0}^{t_f} \| (y(s) - \bar{y}) - P (y(s) - \bar{y}) \|_2^2 \, ds \, .$$

The solution to this problem requires the construction of the correlation matrix

$$R = \int_{t_0}^{t_f} (y(s) - \bar{y}) (y(s) - \bar{y})^T \, ds \, .$$

If $\lambda_1 \geq \lambda_2 \geq \cdots \geq \lambda_m \geq 0$ are the ordered eigenvalues of the symmetric positive semidefinite matrix R, then the minimum value of d^2 over all k-dimensional affine subspaces S passing through $\bar{y}$ is given by $\sum_{j=k+1}^{n} \lambda_j$. As before, the minimizing S is the invariant subspace corresponding to the eigenvalues $\lambda_1, \ldots, \lambda_k$, while the projection matrix ρ consistes of the unit eigenvectors corresponding to these k largest eigenvalues.

Since the square distance d^2 is nothing but the L_2 norm of the projection error, we can readily obtain the following bound on $||e_\perp||_{L_\infty}$:

$$||e_\perp||_{L_\infty} \leq ||e_\perp||_{L_2} \equiv \sqrt{\sum_{j=k+1}^{n} \lambda_j} \, .$$

In practice, of course, the above integrals are approximated from data at discrete times. It is easy to see that using a trapezoidal approximation on a regular grid will lead to the same subspace S as the one obtained with the POD definition in §2.1, while the corresponding optimal total square distances will be proportional.

NOTE. We use the following definition for the L_p norm ($p \geq 1$) of a vector-valued function $f : [t_0, t_f] \to \mathbb{R}^N$:

$$||f||_{L_p} = \left(\int_{t_0}^{t_f} ||f(s)||_p^p \, ds \right)^{1/p} ,$$
$$\text{where } ||f(s)||_p = \left(\sum_{i=1}^{N} |f_i(s)|^p \right)^{1/p} .$$

In particular,

$$||f||_{L_1} = \int_{t_0}^{t_f} \sum_{i=1}^{N} |f_i(s)| \, ds \, ,$$
$$||f||_{L_\infty} = \text{ess sup} \left(\max_i |f_i(s)| \right) .$$

With the above norm definitions, the inequality in (17) is nothing but Hölder's inequality

$$||f^T g||_{L_1} \leq ||f||_{L_p} \cdot ||g||_{L_q} \, , \quad \text{if } \frac{1}{p} + \frac{1}{q} = 1 \, , \tag{19}$$

extended to vector-valued functions f and g, for $p = 1$ and $q = \infty$.

4 Regions of validity for POD-reduced models

Typically, once a reduced model is constructed, we wish to apply it to simulate systems that are close in some sense to the system that was used for generating the reduced model. This raises the issue of estimating approximation errors to help define the range over which the reduced model can be used with acceptable accuracy.

Let $Y \in \mathbb{R}^n$ be the solution of an ODE obtained by applying some perturbation to (1), either in the initial conditions (in which case we use the notation $Y^{\rm ic}$) or in the right-hand side (in which case we use the notation $Y^{\rm rhs}$). The goal here is to estimate the errors introduced by this perturbation, in addition to the model reduction error $e(t)$. There are two perspectives from which this problem can be addressed:

- First, assume we are given a POD projection matrix, built using the solution of the unperturbed ODE (1), and suppose we are interested in using a reduced model to approximate the perturbed solution Y. Then we want to estimate the error $E^1 = \hat{Y} - Y$, where $\hat{Y}$ is the solution of an ODE of the form (4) for Y, with P based on y.
- Alternatively, we may want estimates for the cummulative error (due to the POD model-reduction and the perturbation in the original ODE); i.e., $E^2 = \hat{Y} - y$, where $\hat{Y}$ is the solution of a POD reduced-model based on the solution Y of the perturbed ODE. To avoid introducing new POD projection matrices and unnecessarily complicate the notation, we will look at the completely equivalent problem of estimating $E^2 = \hat{y} - Y$ (in other words we consider y as being a perturbation to Y).

In the rest of this section we derive estimates for E_1 and E_2 considering first a perturbation to the initial condition of the original ODE and then a perturbation to its right-hand side, through some model parameters p.

First, let us define the perturbed ODE systems under consideration. Let $Y^{\rm ic} \in \mathbb{R}^n$ satisfy the evolution equation (1), but with a perturbed initial condition

$$\frac{dY^{\rm ic}}{dt} = f(Y^{\rm ic}, t)\,, \quad Y^{\rm ic}(t_0) = Y_0^{\rm ic} = y_0 + \delta y_0\ . \tag{20}$$

Using the same POD projection matrix P as before, a reduced model corresponding to (20), expressed in the full coordinate system, is given by

$$\frac{d\hat{Y}^{\rm ic}}{dt} = Pf(\hat{Y}^{\rm ic}, t)\,, \quad \hat{Y}^{\rm ic}(t_0) = P(Y_0^{\rm ic} - \bar{y}) + \bar{y}\ . \tag{21}$$

The solutions of the original and perturbed ODEs, as well as the errors e, E_1 and E_2, for this situation are illustrated in Fig. 2(a).

If the original evolution equation depends, through its defining function f, on some model parameters $p \in \mathbb{R}^{N_p}$:

$$\frac{dy}{dt} = f(y, t, p)\,, \quad y(t_0) = y_0\ . \tag{22}$$

then the solution $Y^{\rm rhs}$ corresponding to a perturbation δp in p satisfies

$$\frac{dY^{\rm rhs}}{dt} = f(Y^{\rm rhs}, t, p + \delta p)\,, \quad Y^{\rm rhs}(t_0) = y_0\,. \tag{23}$$

Let $\hat{Y}^{\rm rhs}$ be the solution of the POD-reduced model

$$\frac{d\hat{Y}^{\rm rhs}}{dt} = Pf(\hat{Y}^{\rm rhs}, t, p + \delta p)\,, \quad \hat{Y}^{\rm rhs}(t_0) = P(y_0 - \bar{y}) + \bar{y}\ ,$$

where P is the POD projection matrix constructed with data obtained from (22), i.e., with $\delta p = 0$. The error components for this situation are illustrated in Fig. 2(b).

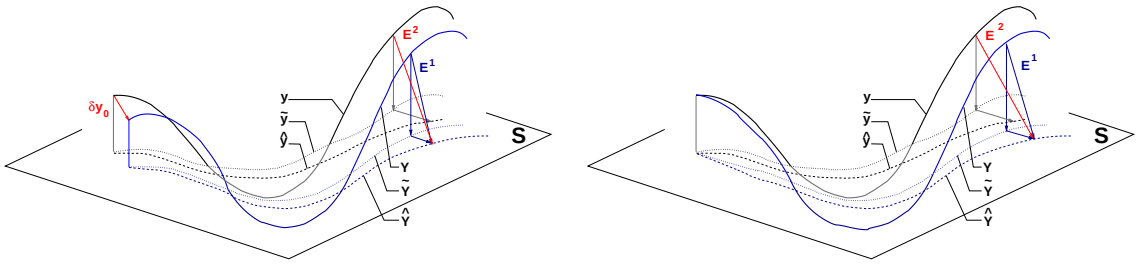

(a) Perturbation in initial conditions.

(b) Perturbation in right-hand side.

Figure 2: Error components in model-reduction of perturbed systems. The solution of the perturbed system, its projection onto S, and the solution of the reduced perturbed system are denoted with Y, $\tilde{Y}$, and $\hat{Y}$, respectively. The error E_1 represents the error commited in reducing the perturbed model, while E_2 is the cummulative error (perturbation + model-reduction)

NOTE. *Useful* estimates should not rely on the solution Y (or $\hat{Y}$) of the perturbed system (or its POD-reduction). Indeed, such error estimates are desired with the sole objective of deciding whether or not to solve these systems.

4.1 Perturbation in initial conditions

4.1.1 Estimation of $E^1 = \hat{Y}^{\mathbf{ic}} - Y^{\mathbf{ic}}$

In this case, we are interested in expressing the relationship between $E^1(t) = \hat{Y}^{\rm ic}(t) - Y^{\rm ic}(t)$ and δy_0. It is obvious that an SCE estimate like (10) is not useful in the sense described above, as it would be based on the error equation

$$\frac{dE^1}{dt} = \mathbf{J}(\hat{Y}^{\rm ic}, t)E^1 - (I-P)f(\hat{Y}^{\rm ic}, t)\,, \quad E^1(t_0) = -(I-P)(y_0 + \delta y_0 - \bar{y})\,, \tag{24}$$

which is a linearization around the (unknown) trajectory $\hat{Y}^{\rm ic}(t)$.

Instead, let us define $\Delta^{\rm ic}(t) = E^1(t) - e(t)$. The norm $\|E^1(t_f)\|$ can be bounded by

$$\big|\|e(t_f)\| - \|\Delta^{\rm ic}(t_f)\|\big| \le \|E^1(t_f)\| \le \|e(t_f)\| + \|\Delta^{\rm ic}(t_f)\|\,.$$

Any estimates of $\|\Delta^{\rm ic}(t_f)\|$ would again require first solving the POD-reduced perturbed system (21). However, following the same idea as in §3.2, this problem can be circumvented by splitting the error $\Delta^{\rm ic}$ into two components: $\Delta^{\rm ic}_\perp$ orthogonal to S and $\Delta^{\rm ic}_i$ parallel to S, as follows

$$\begin{aligned} &\Delta^{\rm ic} = \Delta^{\rm ic}_\perp + \Delta^{\rm ic}_i\ , \\ \text{where}\quad &\Delta^{\rm ic}_\perp = E^1_\perp - e_\perp = (\tilde{Y}^{\rm ic} - Y^{\rm ic}) - (\tilde{y} - y) = -(I-P)(Y^{\rm ic} - y) \\ &\Delta^{\rm ic}_i = E^1_i - e_i = (\hat{Y}^{\rm ic} - \tilde{Y}^{\rm ic}) - (\hat{y} - \tilde{y}) = (\hat{Y}^{\rm ic} - \hat{y}) - P(Y^{\rm ic} - y) \end{aligned} \tag{25}$$

Next we evaluate the influence of δy_0 on each component separately.

Expanding $\Delta^{\rm ic}_\perp$ in a Taylor series around $\delta y_0 = 0$ and retaining only the first order term, we get

$$\Delta^{\rm ic}_\perp = -(I-P)\left.\frac{dY^{\rm ic}}{d\delta y_0}\right|_{\delta y_0 = 0} \delta y_0\ ,$$

where we have used the fact that $\Delta_\perp^{\rm ic} = 0$ for $\delta y_0 = 0$. Let $\Psi^{\rm ic}$ denote the sensitivity matrix $dY^{\rm ic}/dy_0$. Direct differentiation of (20) with respect to δy_0 leads to the following sensitivity equation for $\Psi^{\rm ic}$:

$$\frac{d\Psi^{\rm ic}}{dt} = \mathbf{J}(y,t)\Psi^{\rm ic}\,, \quad \Psi^{\rm ic}(t_0) = I\,.$$

In the above equation, the Jacobian must be evaluated at $\delta y_0 = 0$, in which case $Y^{\rm ic} \equiv y$. The sensitivity matrix $\Psi^{\rm ic}$ is therefore nothing but the fundamental matrix corresponding to the ODE (1), i.e., Φ_y. Therefore, if λ_y is solution of the adjoint system

$$\frac{d\lambda_y}{dt} = -\mathbf{J}^T(y,t)\lambda_y\,, \quad \lambda_y(t_f) = (I-P)z\,, \tag{26}$$

for a uniformly selected random vector $z \in \mathbb{S}_{n-1}$, it is easy to see that

$$z^T\Delta_\perp^{\rm ic}(t_f) = z^T\left[-(I-P)\Psi^{\rm ic}(t_f)\delta y_0\right] = -\lambda_y^T(t_0)\cdot\delta y_0\,, \tag{27}$$

where we have used that $(I-P)^T = (I-P)$.

Equations (26) and (27) can be used with the SCE method by uniformly and randomly selecting z from the sphere $\mathbb{S}_{n-1}$ and then projecting them onto $S^\perp$, the orthogonal complement of S, to initialize the adjoint system (26). However, this does not take into account the fact that $\Delta_\perp^{\rm ic}$ is orthogonal to S. A more accurate estimate can be obtained by using vectors from the sphere $\mathbb{S}_{n-k-1}$ embeded in $S^\perp$. If z' is the representation in $\mathbb{R}^n$ of such a vector, then $(I-P)z' = z'$. The same adjoint system (26) and formula (27) can be used, but the probability that the estimate lies within a given factor w of the true norm $\|\Delta_\perp^{\rm ic}(t_f)\|$ is now higher (see the note in §2.2 for a numerical illustration). For a more efficient estimate, in practice we use the approximation $y \approx \hat{y}$ in evaluating the Jacobian in (26), with $\hat{y}$ computed from the solution y^S of the k-dimensional ODE (3).

Therefore, an SCE estimate of the norm of $\Delta_\perp^{\rm ic}(t_f)$ is

$$||\Delta_\perp^{\rm ic}(t_f)|| \approx \frac{W_q}{W_n}\left[\sum_{j=1}^{q}|{z'}_j^T\Delta_\perp^{\rm ic}(t_f)|^2\right]^{1/2} = \frac{W_q}{W_n}\left[\sum_{j=1}^{q}|\lambda_{\hat{y}}^T(t_0)\delta y_0|^2\right]^{1/2}, \tag{28}$$

where $\lambda_{\hat{y}}$ is the solution of

$$\frac{d\lambda_{\hat{y}}}{dt} = -\mathbf{J}^T(\hat{y},t)\lambda_{\hat{y}}\,, \quad \lambda_{\hat{y}}(t_f) = (I-P)z'_j\,.$$

A direct application of Hölder's inequality (with $p = q = 2$) gives

$$|\lambda_{\hat{y}}^T(t_0)\delta y_0| \le ||\lambda_{\hat{y}}(t_0)||_2\cdot||\delta y_0||_2$$

and therefore

$$||\Delta_\perp^{\rm ic}(t_f)|| \le \kappa(\Delta_\perp^{\rm ic})\cdot||\delta y_0||\,,$$

where the "condition number" for the orthogonal component of $\Delta^{\rm ic}$ is defined as

$$\kappa(\Delta_\perp^{\rm ic}) = \frac{W_q}{W_n}\left[\sum_{j=1}^{q}\kappa_j^2(\Delta_\perp^{\rm ic})\right]^{1/2}, \quad \kappa_j(\Delta_\perp^{\rm ic}) = ||\lambda_{\hat{y}}(t_0)||_2\,.$$

Differentiating with respect to time the expression of $\Delta_i^{\rm ic}$ in (25) and substituting the appropriate ODE right hand sides, we get

$$\frac{d\Delta_i^{\rm ic}}{dt} = \Big(Pf(\hat{Y}^{\rm ic},t) - Pf(\hat{y},t)\Big) - P\left(f(Y^{\rm ic},t) - f(y,t)\right) \approx P\mathbf{J}(\hat{y},t)(\hat{Y}^{\rm ic}-\hat{y}) - P\mathbf{J}(y,t)(Y^{\rm ic}-y)\,,$$

where we have used first order approximations, around $\hat{y}$ for the first half and around y for the second half. Approximating the Jacobian at y by its value evaluated at $\hat{y}$, i.e., $\mathbf{J}(y,t) \approx \mathbf{J}(\hat{y},t)$, we get

$$\frac{d\Delta_i^{\rm ic}}{dt} = P\mathbf{J}(\hat{y},t)\Delta_i^{\rm ic} \ .$$

Since at the initial time ${E^1}_i(t_0) = e_i(t_0) = 0$, we have that $\Delta_i^{\rm ic}(t_0) = 0$ and therefore, in a first order approximation, $\Delta_i^{\rm ic}(t) = 0$, for any $t \geq 0$. In other words, a perturbation to the initial conditions of the original ODE does not introduce additional subspace integration errors.

From the above derivation it follows that $\Delta^{\rm ic}(t_f) \approx \Delta_\perp^{\rm ic}(t_f)$ and therefore

$$\left| \|e(t_f)\| - \|\Delta_\perp^{\rm ic}(t_f)\| \right| \ \leq \ \|E^1(t_f)\| \ \leq \ \|e(t_f)\| + \|\Delta_\perp^{\rm ic}(t_f)\| \ \leq \ \|e(t_f)\| + \kappa(\Delta_\perp^{\rm ic}) \cdot ||\delta y_0|| \, . \tag{29}$$

NOTE. When using SCE estimates for the norms involved in the above bounds, the true value of $\|E^1(t_f)\|$ may not be bracketed by these bounds.

4.1.2 Estimation of $E^2 = \hat{y} - Y^{\rm ic}$

Following the same reasoning as in §3.1, we first derive an ODE satisfied by the error $E^2 = \hat{y} - Y^{\rm ic}$. Subtracting the ODEs satisfied by $\hat{y}$ and $Y^{\rm ic}$, we have

$$\frac{dE^2}{dt} = Pf(\hat{y},t) - f(Y^{\rm ic},t) = Pf(\hat{y},t) - f(\hat{y},t) + f(\hat{y},t) - f(Y^{\rm ic},t) \approx \mathbf{J}(\hat{y},t)E^2 - (I-P)f(\hat{y},t) \, ,$$

where the initial condition for E^2 is given by

$$E^2(t_0) = \hat{y}(t_0) - Y^{\rm ic}(t_0) = (P(y_0 - \bar{y}) + \bar{y}) - (y_0 + \delta y_0) = -(I-P)(y_0 - \bar{y}) - \delta y_0 \, .$$

Therefore to a first order approximation, E^2 satisfies

$$\frac{dE^2}{dt} = \mathbf{J}(\hat{y},t)E^2 - (I-P)f(\hat{y},t) \, , \quad E^2(t_0) = -(I-P)(y_0 - \bar{y}) - \delta y_0 \, . \tag{30}$$

With $\lambda_{\hat{y}}$ the solution of the adjoint system (9) and for some random vector z uniformly selected from the unit sphere $\mathbb{S}_{n-1}$ we have

$$\begin{aligned} z^T E^2(t_f) &= -\int_{t_0}^{t_f} \lambda_{\hat{y}}^T(s)(I-P)f(\hat{y}(s),s)\, ds - \lambda_{\hat{y}}^T(t_0)\left((I-P)(y_0 - \bar{y}) + \delta y_0\right) \\ &= z^T e(t_f) - \lambda_{\hat{y}}^T(t_0)\delta y_0 \, , \end{aligned} \tag{31}$$

where $e(t_f)$ is the approximation error for the original system, defined by (6). Comparing the above equation with (27), we conclude that

$$z^T E^2(t_f) = z^T \left[e(t_f) + \Gamma^{\rm ic}(t_f) \right] \, , \tag{32}$$

where $\Gamma^{\rm ic}(t) \triangleq \Psi_{\hat{y}}^{\rm ic}(t)\delta y_0$, and the matrix $\Psi_{\hat{y}}^{\rm ic}$ is the solution of

$$\frac{d\Psi_{\hat{y}}^{\rm ic}}{dt} = \mathbf{J}(\hat{y},t)\Psi_{\hat{y}}^{\rm ic} \, , \quad \Psi_{\hat{y}}^{\rm ic}(t_0) = I_n \, .$$

Thus, the following inequalities hold:

$$\left| \|e(t_f)\| - \|\Gamma^{\rm ic}(t_f)\| \right| \ \leq \ \|E^2(t_f)\| \ \leq \ \|e(t_f)\| + \|\Gamma^{\rm ic}(t_f)\| \ \leq \ \|e(t_f)\| + \kappa(\Gamma^{\rm ic}) \cdot ||\delta y_0|| \, , \tag{33}$$

where

$$||\Gamma^{\rm ic}(t_f)|| \approx \frac{W_q}{W_n}\left[\sum_{j=1}^{q} |\lambda_{\hat{y}}^T(t_0)\delta y_0|^2\right]^{1/2} \quad \text{and} \quad \kappa(\Gamma^{\rm ic}) = \frac{W_q}{W_n}\left[\sum_{j=1}^{q} \|\lambda_{\hat{y}}(t_0)\|_2^2\right]^{1/2} \, ,$$

with $\lambda_{\hat{y}}$ the solution of (9).

NOTE. Since the equality (32) holds for any vector z and for any final time t_f, we conclude that $E^2 = e + \Gamma^{\rm ic}$, for any t. This is a strict equality, unlike $E^1 \approx e + \Delta_\perp^{\rm ic}$ which is only an approximation (ignoring $\Delta_i^{\rm ic}$ and using $y \approx \hat{y}$ in the adjoint system). As a consequence, the above SCE bound estimates for the norm of $E^2(t_f)$ are more accurate than those derived in §4.1.1 for the norm of $E^1(t_f)$. Furthermore, starting from (31), an SCE estimate for $\|E^2(t_f)\|$ can be computed without need for $Y^{\rm ic}$ or $\hat{Y}^{\rm ic}$.

4.2 Perturbation in the right hand side

4.2.1 Estimation of $E^1 = \hat{Y}^{\mathbf{rhs}} - Y^{\mathbf{rhs}}$

Following the same arguments as in §4.1.1, we treat directly the case in which we decompose the error $\Delta^{\rm rhs} = E^1 - e$ into its components $\Delta_\perp^{\rm rhs} \in S^\perp$ and $\Delta_i^{\rm rhs} \in S$.

As before, we start with a Taylor expansion of $\Delta_\perp^{\rm rhs}$ around $\delta p = 0$ and retain only the first order term:

$$\Delta_\perp^{\rm rhs} = -(I - P)\, \frac{dY^{\rm rhs}}{d\delta p}\bigg|_{\delta p = 0} \delta p \ .$$

With $\Psi^{\rm rhs}$ the sensitivity matrix $dY^{\rm rhs}/dp$, we have

$$\frac{d\Psi^{\rm rhs}}{dt} = \mathbf{J}(y,t,p)\Psi^{\rm rhs} + \mathbf{K}(y,t,p)\,, \quad \Psi^{\rm rhs}(t_0) = 0\,,$$

where $\mathbf{K} = \partial f/\partial p$. The solution $\Psi^{\rm rhs}$ of this matrix sensitivity system can be written in terms of the fundamental matrix Φ_y as

$$\Psi^{\rm rhs}(t_f) = \int_{t_0}^{t_f} \Phi_y(t_f)(\Phi_y(s))^{-1}\mathbf{K}(y(s),s,p)\, ds \ .$$

For an arbitrary $z \in \mathbb{R}^n$, the product $z^T\Delta_\perp^{\rm rhs}(t_f)$ can then be obtained from the solution λ_y of the adjoint system (26) as

$$z^T\Delta_\perp^{\rm rhs}(t_f) = -\left(\int_{t_0}^{t_f} \lambda_y^T(s)\mathbf{K}(y(s),s,p)\, ds\right)\cdot \delta p \ . \tag{34}$$

The same observations as before apply here too: (1) a more accurate SCE error norm estimate can be obtained if using vectors z' from the $\mathbb{S}_{n-k-1}$ sphere embedded in $S^\perp$; and (b) a more efficient adjoint solution can be obtained by approximation $y \approx \hat{y}$ for the evaluation of $\mathbf{J}(y,t,p)$ and $\mathbf{K}(y,t,p)$. Therefore, the norm of $\Delta_\perp^{\rm rhs}$ can be estimated by

$$||\Delta_\perp^{\rm rhs}(t_f)|| \approx \frac{W_q}{W_n}\left[\sum_{j=1}^{q} |{z'}_j^T\Delta_\perp^{\rm rhs}(t_f)|^2\right]^{1/2} = \frac{W_q}{W_n}\left[\sum_{j=1}^{q}\left|\int_{t_0}^{t_f}\lambda_{\hat{y}}^T(s)\mathbf{K}(\hat{y}(s),s,p)\,\delta p\, ds\right|^2\right]^{1/2}, \tag{35}$$

or bounded by

$$||\Delta_\perp^{\rm rhs}(t_f)|| \le \kappa(\Delta_\perp^{\rm rhs})\cdot||\delta p||_\infty\,,$$

where the "condition number" $\kappa(\Delta_\perp^{\rm rhs})$ is defined as

$$\kappa(\Delta_\perp^{\rm rhs}) = \frac{W_q}{W_n}\left[\sum_{j=1}^{q}\kappa_j^2(\Delta_\perp^{\rm rhs})\right], \quad \kappa_j(\Delta_\perp^{\rm rhs}) = ||\lambda_{\hat{y}}^T\mathbf{K}||_{L_1}\,.$$

The differential equation satisfied by the component $\Delta_i^{\rm rhs}$ parallel to S is given by

$$\frac{d\Delta_i^{\rm rhs}}{dt} = \Big(Pf(\hat{Y}^{\rm rhs}, t, p+\delta p) - Pf(\hat{y}, t, p)\Big) - P\left(f(Y^{\rm rhs}, t, p+\delta p) - f(y, t, p)\right)$$
$$\approx P\left(\mathbf{J}(\hat{y}, t, p)(\hat{Y}^{\rm rhs} - \hat{y}) + \mathbf{K}(\hat{y}, t, p)\,\delta p\right) - P\left(\mathbf{J}(y, t)(Y^{\rm rhs} - y) + \mathbf{K}(y, t, p)\,\delta p\right) \ ,$$

with $\mathbf{K}$ defined as above. With the approximations $\mathbf{J}(y, t, p) \approx \mathbf{J}(\hat{y}, t, p)$ and $\mathbf{K}(y, t, p) \approx \mathbf{K}(\hat{y}, t, p)$, we obtain

$$\frac{d\Delta_i^{\rm rhs}}{dt} = P\mathbf{J}(\hat{y}, t, p)\Delta_i^{\rm rhs} \ .$$

As before, $\Delta_i^{\rm rhs}(t_0) = 0$ and therefore, in a first order approximation, $\Delta_i^{\rm rhs}(t) = 0$, for any $t \geq 0$.

From the above derivation it follows that $\Delta^{\rm rhs}(t_f) \approx \Delta_\perp^{\rm rhs}(t_f)$ and therefore

$$\big|\|e(t_f)\| - \|\Delta_\perp^{\rm rhs}(t_f)\|\big| \ \leq \ \|E^1(t_f)\| \ \leq \ \|e(t_f)\| + \|\Delta_\perp^{\rm rhs}(t_f)\| \ \leq \ \|e(t_f)\| + \kappa(\Delta_\perp^{\rm rhs}) \cdot ||\delta p||_\infty \, . \quad (36)$$

with $\|\Delta_\perp^{\rm rhs}(t_f)\|$ given by (35).

4.2.2 Estimation of $E^2 = \hat{y} - Y^{\rm rhs}$

An ODE satisfied by the error $E^2 = \hat{y} - Y^{\rm rhs}$ can be obtained as in §4.1.2. Substituting the right hand sides of the ODEs satisfied by $\hat{y}$ and $Y^{\rm rhs}$, and explicitely taking into account the dependence of f on the model parameters p, we have

$$\frac{dE^2}{dt} = Pf(\hat{y}, t, p) - f(Y^{\rm rhs}, t, p+\delta p) = Pf(\hat{y}, t, p) - f(\hat{y}, t, p) + f(\hat{y}, t, p) - f(Y^{\rm rhs}, t, p+\delta p)$$
$$\approx \mathbf{J}(\hat{y}, t, p)E^2 - (I-P)f(\hat{y}, t, p) - \mathbf{K}(\hat{y}, t, p)\,\delta p \, ,$$

and

$$E^2(t_0) = \hat{y}(t_0) - Y^{\rm rhs}(t_0) = (P(y_0 - \bar{y}) + \bar{y}) - y_0 = -(I-P)(y_0 - \bar{y}) \, .$$

Therefore, to a first order approximation, E^2 satisfies

$$\frac{dE^2}{dt} = \mathbf{J}(\hat{y}, t, p)E^2 - (I-P)f(\hat{y}, t, p) - \mathbf{K}(\hat{y}, t, p)\,\delta p \, , \quad E^2(t_0) = -(I-P)(y_0 - \bar{y}) \, . \quad (37)$$

For $\lambda_{\hat{y}}$ the solution of the adjoint system (9) and some random vector z uniformly selected from the unit sphere $\mathbb{S}_{n-1}$, we have

$$\begin{aligned} z^T E^2(t_f) &= -\int_{t_0}^{t_f} \lambda_{\hat{y}}^T(s)\left[(I-P)f(\hat{y}(s), s, p) + \mathbf{K}(\hat{y}(s), s, p)\,\delta p\right] ds - \lambda_{\hat{y}}^T(t_0)(I-P)(y_0 - \bar{y}) \\ &= z^T e(t_f) - \int_{t_0}^{t_f} \lambda_{\hat{y}}^T(s)\mathbf{K}(\hat{y}(s), s, p)\,\delta p\, ds \, , \end{aligned} \quad (38)$$

where $e(t_f)$ is the approximation error for the original system, defined by (6).

As in §4.1.2, we can write $E^2 = e + \Gamma^{\rm rhs}$, with $\Gamma^{\rm rhs}(t) \triangleq \Psi_{\hat{y}}^{\rm rhs}(t)\,\delta p$ and

$$\frac{d\Psi_{\hat{y}}^{\rm rhs}}{dt} = \mathbf{J}(\hat{y}, t, p)\Psi_{\hat{y}}^{\rm rhs} + \mathbf{K}(\hat{y}, t, p) \, , \quad \Psi_{\hat{y}}^{\rm rhs}(t_0) = 0 \, .$$

Therefore, the following inequalities hold:

$$\big|\|e(t_f)\| - \|\Gamma^{\rm rhs}(t_f)\|\big| \ \leq \ \|E^2(t_f)\| \ \leq \ \|e(t_f)\| + \|\Gamma^{\rm rhs}(t_f)\| \ \leq \ \|e(t_f)\| + \kappa(\Gamma^{\rm rhs}) \cdot \|\delta p\|_\infty \, , \quad (39)$$

where

$$||\Gamma^{\rm rhs}(t_f)|| \approx \frac{W_q}{W_n}\left[\sum_{j=1}^{q}\left|\int_{t_0}^{t_f} \lambda_{\hat{y}}^T(s)\mathbf{K}(\hat{y}(s), s, p)\,\delta p\, ds\right|^2\right]^{1/2} \quad \text{and} \quad \kappa(\Gamma^{\rm rhs}) = \frac{W_q}{W_n}\left[\sum_{j=1}^{q}\|\lambda_{\hat{y}}^T\mathbf{K}\|_{L_1}^2\right]^{1/2} \, ,$$

with $\lambda_{\hat{y}}$ the solution of (9).

NOTE. The above SCE bound estimates for the norm of $E^2(t_f)$ are more accurate than those derived in §4.2.1 for the norm of $E^1(t_f)$. Furthermore, starting from (38), an SCE estimate for $\|E^2(t_f)\|$ can be computed without need for Y^{rhs} or $\hat{Y}^{\text{rhs}}$.

5 Examples

To illustrate the norm estimates and bounds derived in the previous sections, we consider the following five example problems (described in more detail below): (a) linear advection-diffusion PDE; (b) Burgers' PDE; (c) Brusselator PDE; (d) HIRES (High Irradiance Response) problem; and (e) a pollution model.

Numerical Results. For each example considered, we provide numerical results grouped in three figures:

1. Estimation of the POD approximation error as a function of the dimension of the subspace S.

   (a) $\|e(t_f)\|$, the norm of the total approximation error at the final time, $e(t_f) = \hat{y}(t_f) - y(t_f)$. The solid (black) line represents the norm computed by the forward integration of the error equation (7). The dotted (colored) lines represent SCE estimates (10) for different values of q, the number of unit vectors z_j used.

   (b) $\|e_i^S(t_f)\|$, the norm of the subspace integration error at the final time, computed in the subspace S. The solid (black) line represents the norm computed by the forward integration of the error equation (14). The dotted (colored) lines represent SCE estimates (16) for different values of q. The dashed (colored) lines represent the bounds of (18) for different values of q used in the estimation of the condition number $\kappa(e_i)$.

2. Estimation of errors induced by a perturbation δy_0 in the initial conditions.

   (a) $\|E^1(t_f)\|$, the norm of the total approximation error of the perturbed system at the final time, $E^1(t_f) = \hat{Y}^{\text{ic}}(t_f) - Y^{\text{ic}}(t_f)$, as a function of the subspace dimension N_k. The solid (black) line represents the norm computed by the forward integration of the error equation (24). The dashed (colored) lines represent SCE estimates of the upper bound of (29) for different values of q used in the estimation of the condition number $\kappa(\Delta_\perp^{\text{ic}})$. Note that we have also used an SCE estimate for the norm $\|e(t_f)\|$.

   (b) $\|E^2(t_f)\|$, the norm of the cumulative error of the perturbed system at the final time, $E^2(t_f) = \hat{y}(t_f) - Y^{\text{ic}}(t_f)$, as a function of the subspace dimension N_k. The solid (black) line represents the norm computed by the forward integration of the error equation (30). The dotted (colored) lines represent SCE estimates for the norm $\|E^2(t_f)\|$ for different values of q. The dashed (colored) lines represent SCE estimates of the upper bound of (33) for different values of q used in the estimation of the condition number $\kappa(\Gamma^{\text{ic}})$. Note that we have also used an SCE estimate for the norm $\|e(t_f)\|$.

   (c) Analysis of the error bounds for $\|E^1(t_f)\|$ predicted by the condition number $\kappa(\Delta_\perp^{\text{ic}})$ over a range of initial condition perturbations δy_0, for a given dimension N_k of the subspace S. The solid (black) line represents the norm computed by the forward integration of the error equation (24), while the dashed (colored) lines represent the upper bounds of (29).

   (d) Analysis of the error bounds for $\|E^2(t_f)\|$ predicted by the condition number $\kappa(\Gamma^{\text{ic}})$ over a range of initial condition perturbations δy_0, for a given dimension N_k of the subspace S. The solid (black) line represents the norm computed by the forward integration of the error equation (30), while the dashed (colored) lines represent the upper bounds of (33).

3. Estimation of errors induced by a perturbation in the ODE right hand side (through a perturbation δp in the model parameters).

   (a) $\|E^1(t_f)\|$, the norm of the total approximation error of the perturbed system at the final time, $E^1(t_f) = \hat{Y}^{\text{rhs}}(t_f) - Y^{\text{rhs}}(t_f)$, as a function of the subspace dimension N_k. The solid (black) line represents the norm computed by the forward integration of the error equation. The dashed (colored) lines represent SCE estimates of the upper bound of (36) for different values of q used in the estimation of the condition number $\kappa(\Delta_{\perp}^{\text{rhs}})$. Note that we have also used an SCE estimate for the norm $\|e(t_f)\|$.

   (b) $\|E^2(t_f)\|$, the norm of the cumulative error of the perturbed system at the final time, $E^2(t_f) = \hat{y}(t_f) - Y^{\text{rhs}}(t_f)$, as a function of the subspace dimension N_k. The solid (black) line represents the norm computed by the forward integration of the error equation (37). The dotted (colored) lines represent SCE estimates for the norm $\|E^2(t_f)\|$ for different values of q. The dashed (colored) lines represent SCE estimates of the upper bound of (39) for different values of q used in the estimation of the condition number $\kappa(\Gamma^{\text{rhs}})$. Note that we have also used an SCE estimate for the norm $\|e(t_f)\|$.

   (c) Analysis of the error bounds for $\|E^1(t_f)\|$ predicted by the condition number $\kappa(\Delta_{\perp}^{\text{rhs}})$ over a range of perturbations δp in the model parameters, for a given dimension N_k of the subspace S. The solid (black) line represents the norm computed by the forward integration of the error equation, while the dashed (colored) lines represent the upper bounds of (36).

   (d) Analysis of the error bounds for $\|E^2(t_f)\|$ predicted by the condition number $\kappa(\Gamma^{\text{rhs}})$ over a range of parameter perturbations δp, for a given dimension N_k of the subspace S. The solid (black) line represents the norm computed by the forward integration of the error equation, while the dashed (colored) lines represent the upper bounds of (39).

The dimension of the POD subspace. Let us denote by Λ_k the sum of eigenvalues ignored in the construction of the POD reduced model

$$\Lambda_k = \sum_{i=k+1} \lambda_i$$

and by Λ its relative size compared to the sum of all eigenvalues

$$\Lambda = \Lambda_k / \sum_{i=1} \lambda_i$$

The POD subspace dimension k is selected such that the relative error is very close to one, yet k is sufficiently small. A relative error near one means that a very high percentage of the energy for the full model was captured by the reduced order model.

An interesting phenomenon can be observed in some of the numerical experiments. Some of the estimates computed for a certain number of POD vectors are not as good as estimates corresponding to a smaller POD subspace dimension. At a first glance this would contradict the theoretical description of the POD method, which implies that the original model would be better approximated as the POD dimension increases. In fact there is no contradiction. If one considers the entire time interval, one can notice that the reduced model captures a larger percentage of the original problem as we add more POD vectors. But our figures show the behavior of the reduced model only at the final time, not over the entire time interval. Therefore we may have that, at certain time points (e.g., the final time) the estimate for a smaller POD dimension is better while also having that the larger POD number would provide a "closer" estimate (in the norm over the entire time interval).

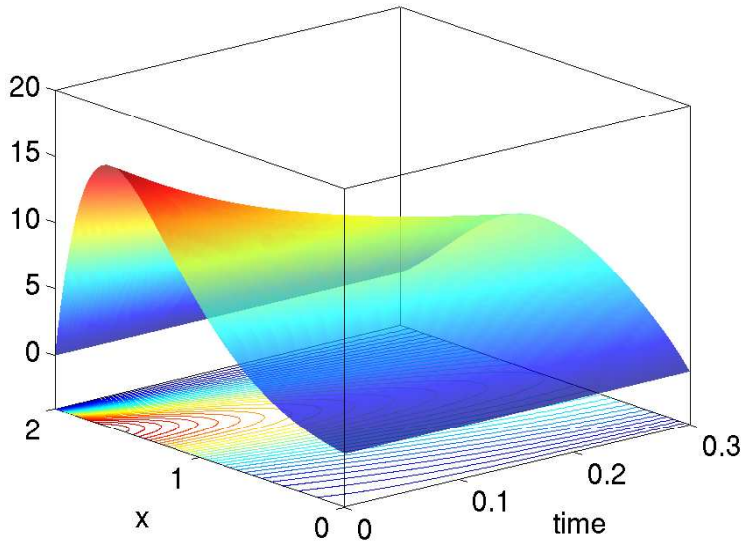

Figure 3: 1D advection-diffusion example. Behavior of the solution over the integration interval.

The number of orthogonal vectors for the SCE estimate. We considered one, two, and three SCE vectors for our numerical examples. As expected, having just one SCE vector yielded the worst estimate in most of the cases. Nevertheless, even that estimate was, in many cases, "close enough" to warrant its inclusion in our results.

5.1 Linear advection-diffusion

Consider the 1-D advection-diffusion equation:

$$\begin{aligned} & u_t = p_1 u_{xx} + p_2 u_x \\ \text{with B.C.} \quad & u(0,t) = u(2,t) = 0 \\ \text{and I.C.} \quad & u(x,0) = u_0(x) = x(2-x)e^{2x} \,. \end{aligned}$$

The PDE is discretized on a uniform grid of size $N+2$ with central differencing. If boundary values are eliminated, that leaves an ODE system of size N

$$\begin{aligned} \frac{dy_i}{dt} &= p_1 \frac{y_{i+1} - 2y_i + y_{i-1}}{\Delta x^2} + p_2 \frac{y_{i+1} - y_{i-1}}{2\Delta x} \\ y_i(0) &= u_0(x_i) \end{aligned}$$

where $y_i(t) = u(x_i, t)$ and $x_i = i * \Delta x$.

A plot showing the solution behavior over the integration domain is presented in Fig. 3. The problem parameters were $p_1 = 0.5$ and $p_2 = 1.0$, while the spatial grid parameter was $N = 100$. Numerical results at $t = 0.3$ are given in Figs. 8, 9, and 10. The POD projection matrices were based on $m = 100$ data points equally spaced in the interval $[t_0, t_f] = [0.00.3]$. The POD errors ($\Lambda_k = \sum_{i=k} \lambda_i$, the sum of ignored eigenvalues) and their relative size compared to the sum of all eigenvalues ($\Lambda = \Lambda_k / \sum \lambda_i$), for all subspace dimensions considered were:

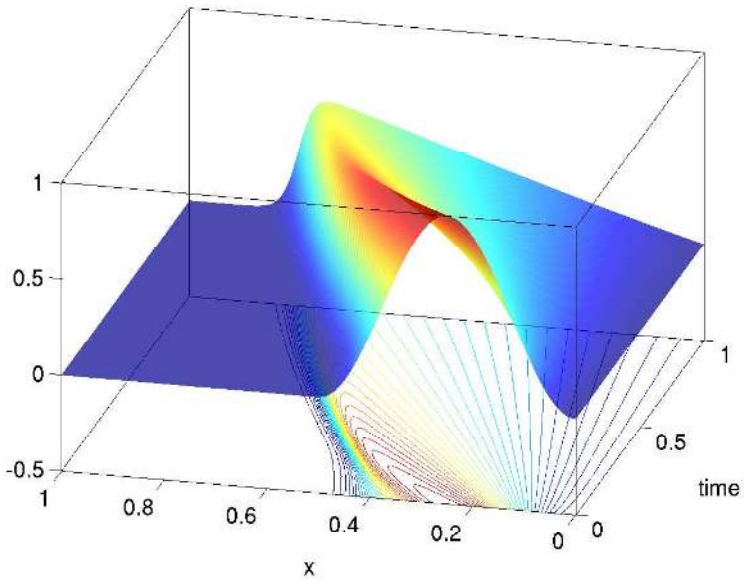

Figure 4: Burger's equation example. Behavior of the solution over the integration interval.

N_k	Λ_k	Λ
5	1.803561e-01	5.890413e-06
6	2.831234e-02	9.246781e-07
7	4.193422e-03	1.369567e-07
8	5.662276e-04	1.849294e-08
9	6.944298e-05	2.268001e-09
10	7.716002e-06	2.520038e-10

The estimate of the total error is consistently "close" to the exact value. Moreover the estimates corresponding to $N_z = 2, 3$ are almost identical to the subspace integration error.

The bounds are within an order of magnitude for both IC and RHS perturbation. The RHS perturbation increases the distance between the bounds and the forward error. That was expected, since the RHS perturbation would change the advection coefficient p_2, which is dominant for the time window considered.

5.2 Burgers' equation

This PDE has the form

$$
\begin{aligned}
& u_t + uu_x = \mu u_{xx} \\
\text{with B.C.} \quad & u(0,t) = u(1,t) = 0 \\
\text{and I.C.} \quad & u(x,0) = u_0(x) = \begin{cases} 0.5(1-\cos 4\pi x) & \text{if } 0 \le x \le 0.5; \\ 0 & \text{if } 0.5 < x \le 1. \end{cases}
\end{aligned}
$$

The PDE is discretized on a uniform grid of size $2N+3$ using central differencing. We eliminate the boundary values to obtain an ODE system of size $2N+1$

$$
\begin{aligned}
\frac{dy_i}{dt} &= \mu \frac{y_{i+1} - 2y_i + y_{i-1}}{\Delta x^2} - y_i \frac{y_{i+1} - y_{i-1}}{2\Delta x} \\
y_i(0) &= u_0(x_i)
\end{aligned}
$$

where $y_i(t) = u(x_i, t)$ and $x_i = i * \Delta x$.

A plot showing the solution behavior over the integration domain is presented in Fig. 4. The problem parameter was $\mu = 0.005$, while the spatial grid parameter was $N = 100$. Numerical results at $t = 1.0$ are given in Figs. 11, 12, and 13. The POD projection matrix were based on $m = 100$ data points equally spaced in the interval $[t_0, t_f] = [0.01.0]$. The POD errors ($\Lambda_k = \sum_{i=k+1} \lambda_i$, the sum of ignored eigenvalues) and their relative size compared to the sum of all eigenvalues ($\Lambda = \Lambda_k / \sum \lambda_i$), for all subspace dimensions considered were:

N_k	Λ_k	Λ
5	1.516695e+01	2.186474e-02
10	8.618580e-01	1.242458e-03
15	5.403372e-02	7.789523e-05
20	3.452479e-03	4.977107e-06

The estimates corresponding to $N_z = 2, 3$ are almost identical to the forward errors. What is surprising is that estimate corresponding to $N_z = 1$ is consistently "close" to the exact error.

As size of the perturbations increases, the behavior of the bounds mimic the behavior of the forward errors, while remaining within an order of magnitude of them.

We note that the forward error is of order $10^{-1} - 10^{0}$. This implies that the truncation errors corresponding to $O(||e||^2)$ are rather large in the POD error equations. Therefore one might expect that the first order approximation employed for the error equations would not yield very accurate estimates and bounds. But the numerical results proved to be better than the expectations. We believe that this is due to the fact that the POD model captures very well the behavior of the original model, as suggested by the data in the above table, showing the relative energy and the total energy.

5.3 Brusselator

The following 1D time-dependent PDE models a chemically reacting system [9]:

$$
\begin{aligned}
& \frac{\partial u}{\partial t} = A + u^2 v - (B+1)u + \alpha \frac{\partial^2 u}{\partial x^2} \\
& \frac{\partial v}{\partial t} = Bu - u^2 v + \alpha \frac{\partial^2 v}{\partial x^2}\,, \\
\text{with B.C.} \quad & u(0,t) = u(1,t) = \bar{A} \\
& v(0,t) = v(1,t) = \bar{B} \\
\text{and I.C.} \quad & u(x,0) = \bar{A} + \sin(2\pi x) \\
& v(x,0) = \bar{B}\,,
\end{aligned}
$$

where $0 \le x \le 1$, $\bar{A} = 1.0$, and $\bar{B} = 3.0$. Using the method of lines, we convert this PDE to an ODE IVP using central finite differences to approximate the space derivatives on a grid of N interior points

$$
\begin{aligned}
& \dot{u}_i = A + u_i^2 v_i - (B+1)u_i + \frac{\alpha}{\Delta x^2}(u_{i-1} - 2u_i + u_{i+1}) \\
& \dot{v}_i = Bu_i + u_i^2 v_i + \frac{\alpha}{\Delta x^2}(v_{i-1} - 2v_i + v_{i+1}) \\
& u_i(0) = A + \sin(2\pi x_i) \\
& v_i(0) = B\,,
\end{aligned}
$$

where $u_i(t) = u(x_i, t)$ and $v_i(t) = v(x_i, t)$, for $i = 1, \ldots, N$ and $x_i = i\Delta x$ with $\Delta x = 1/(N+1)$. The boundary conditions are explicitly used to define $u_0(t) = u(0,t)$, $u_{N+1}(t) = u(1,t)$ and $v_0(t) = v(0,t)$, $v_{N+1}(t) = v(1,t)$.

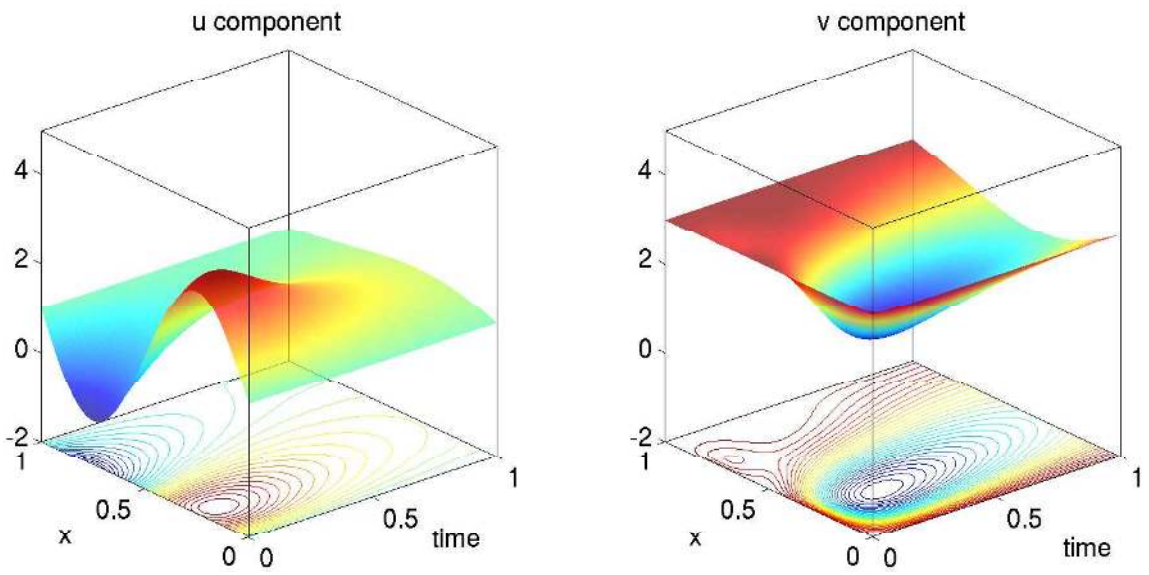

Figure 5: Brusselator example. Behavior of the solution over the integration interval.

A plot showing the solution behavior over the integration domain is presented in Fig. 5. The problem parameters were $A = 1.0$, $B = 3.0$, and $\alpha = 0.1$, while the spatial grid parameter was $N = 50$. Numerical results at $t = 1.0$ are given in Figs. 14, 15, and 16. The POD projection matrix was based on $m = 100$ data points equally spaced in the interval $[t_0, t_f] = [0.01.0]$. The POD errors ($\Lambda_k = \sum_{i=k+1} \lambda_i$, the sum of ignored eigenvalues) and their relative size compared to the sum of all eigenvalues ($\Lambda = \Lambda_k / \sum \lambda_i$), for all subspace dimensions considered were:

N_k	Λ_k	Λ
5	2.421481e-03	2.105985e-06
6	3.394275e-04	2.952033e-07
7	2.932653e-05	2.550556e-08
8	3.970401e-06	3.453096e-09

The total error and the subspace approximation error are well approximated by the estimates corresponding to $N_z = 2, 3$. As N_k increases, the forward error decreases as expected. Moreover the estimates follow it closely, being almost identical at $N_k = 8$.

The bounds for both IC and RHS perturbations are within an order of magnitude of the forward error.

5.4 HIRES problem

HIRES is a stiff system of 8 ODEs described in [9]. It originates from plant physiology and describes how light is involved in morphogenesis. To be more precise, it explains the "High Irradiance Responses' (HIRES) of photomorphogenesis on the basis of phytochrome, by means of a chemical reaction involving eight reactants. The problem is of the form

$$\frac{dy}{dt} = f(y)\,, \quad y(0) = y_0$$

Table 2: Model parameters for the HIRES model

Model parameters				
$k_1 = 1.71$	$k_3 = 8.32$	$k_5 = 0.035$	$k_+ = 280$	$k^* = 0.69$
$k_2 = 0.43$	$k_4 = 0.69$	$k_6 = 8.32$	$k_- = 0.69$	$o_{k_s} = 0.0007$

with $y \in \mathbb{R}^8$ and the function $f(y)$ defined by

$$f(y) = \begin{bmatrix} -k_1 y_1 + k_2 y_2 + k_6 y_3 + o_{k_s} \\ k_1 y_1 - (k_2 + k_3) y_2 \\ -(k_1 + k_6) y_3 + k_2 y_4 + k_5 y_5 \\ k_3 y_2 + k_1 y_3 - (k_2 + k_4) y_4 \\ -(k_1 + k_5) y_5 + k_2 y_6 + k_2 y_7 \\ -k_+ y_6 y_8 + k_4 y_4 + k_1 y_5 - k_2 y_6 + k_- y_7 \\ k_+ y_6 y_8 - (k_2 + k^* + k_-) y_7 \\ -k_+ y_6 y_8 + (k_2 + k^* + k_-) y_7 \end{bmatrix}.$$

Values of the model parameters are given in Table 2. The initial vector is

$$y_0 = [1, 0, 0, 0, 0, 0, 0, 0.0057]^T.$$

A plot showing the solution behavior over the integration domain is presented in Fig. 6. Numerical results at $t = 30.0$ are given in Figs. 17, 18, and 19. We considered a time interval, namely [0,30], that captures the main behavior of the solution (the solution changes at a much slower rate after $t = 30$).

The POD projection matrix was based on $m = 100$ data points equally spaced in the interval $[t_0, t_f] = [0.030.0]$. The POD errors ($\Lambda_k = \sum_{i=k+1} \lambda_i$, the sum of ignored eigenvalues) and their relative size compared to the sum of all eigenvalues ($\Lambda = \Lambda_k / \sum \lambda_i$), for all subspace dimensions considered were:

N_k	Λ_k	Λ
3	6.533327e-03	1.245353e-03
4	1.830350e-04	3.488931e-05
5	8.450097e-07	1.610719e-07

Since this problem is well known in the literature as a good test for stiff systems, our intent (in choosing it) was to verify that our approach can be employed for those type of problems as well.

We note that the total error and the subspace integration error are captured very well by the estimates corresponding to $N_z = 2, 3$. Moreover, as N_k increases, the POD error decreases and the estimates are very closely mirroring that behavior. The problem is very sensitive to perturbations (to both the initial conditions and the RHS). Nevertheless, all the bounds are within an order of magnitude of the forward errors. We did not consider all 10 parameters (Table 2) for the RHS perturbation. We chose a subset $\{k_3, k_4, k_5, k_6\}$ that we considered to contain the most important parameters (one can also consider them as representative for the range of the values for all parameters, namely $10^{-2} - 10^2$).

5.5 Pollution model

Next we consider the chemical reaction part of the air pollution, model developed at the Dutch National Institute of Public Health and Environmental Protection and described by Verwer [28]. It

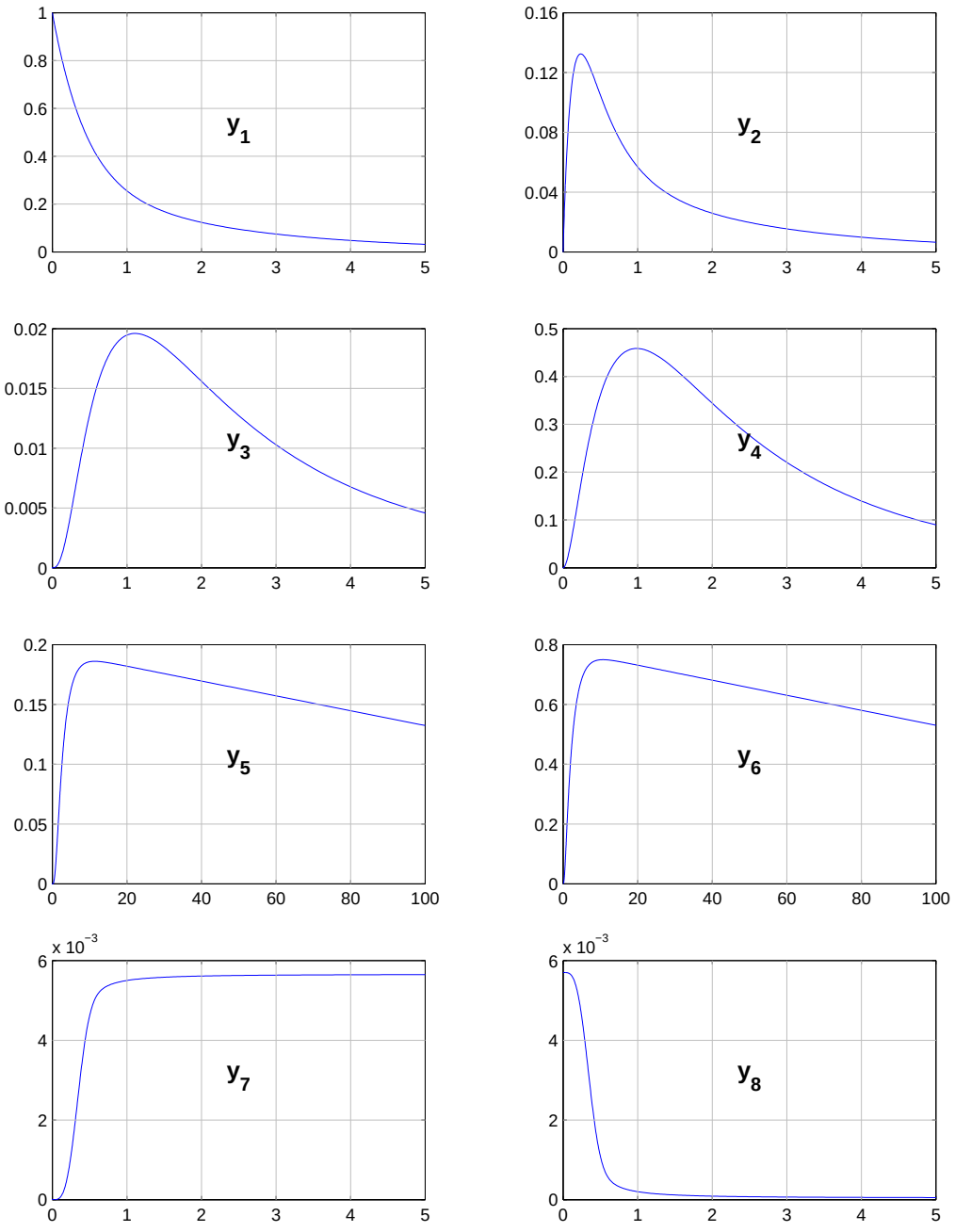

Figure 6: HIRES example. Behavior of the solution over the integration interval.

is a very stiff ODE system consisting of 25 reactions and 20 reacting compounds. The problem is of the form

$$\frac{dy}{dt} = f(y)\,, \quad y(0) = y_0$$

with $y \in \mathbb{R}^{20}$ and the function $f(y)$ defined by

$$f = \begin{bmatrix} -\sum_{j\in\{1,10.14,23,24\}} r_j + \sum_{j\in\{2,3,9,11,12,22,25\}} r_j \\ -r_2 - r_3 - r_9 - r_{12} + r_1 + r_{21} \\ -r_{15} + r_1 + r_{17} + r_{19} + r_{22} \\ -r_2 - r_{16} - r_{17} - r_{23} + r_{15} \\ -r_3 + r_4 + r_4 + r_6 + r_7 + r_{13} + r_{20} \\ -r_6 - r_8 - r_{14} - r_{20} + r_3 + 2r_{18} \\ -r_4 - r_5 - r_6 + r_{13} \\ r_4 + r_5 + r_6 + r_7 \\ -r_7 - r_8 \\ -r_{12} + r_7 + r_9 \\ -r_9 - r_{10} + r_8 + r_{11} \\ r_9 \\ -r_{11} + r_{10} \\ -r_{13} + r_{12} \\ r_{14} \\ -r_{18} - r_{19} + r_{16} \\ -r_{20} \\ r_{20} \\ -r_{21} - r_{22} - r_{24} + r_{23} + r_{25} \\ -r_{25} + r_{24} \end{bmatrix}$$

The values of the auxiliary variables r_j and of the model parameters k_j are given in Table 3. The initial vector is

$$y_0 = [0, 0.2, 0, 0.04, 0, 0, 0.1, 0.3, 0.01, 0.0, 0, 0, 0, 0, 0, 0.007, 0, 0, 0]^T\,.$$

A plot showing the solution behavior over the integration domain is presented in Fig. 7. Numerical results at $t = 1.0$ are given in Figs. 20, 21, and 22. The POD projection matrix was based on $m = 1000$ data points equally spaced in the interval $[t_0, t_f] = [0.01.0]$. The POD errors ($\Lambda_k = \sum_{i=k+1} \lambda_i$, the sum of ignored eigenvalues) and their relative size compared to the sum of all eigenvalues ($\Lambda = \Lambda_k / \sum \lambda_i$), for all subspace dimensions considered were

N_k	Λ_k	Λ
5	6.341930e-13	2.652438e-12
6	6.971282e-14	2.915657e-13
7	1.139176e-15	4.764470e-15
8	1.175776e-16	4.917547e-16
9	4.938977e-17	2.065669e-16
10	9.158667e-18	3.830506e-17

For $N_k = 5, 6, 7$ the total error and the subspace integration error are very well approximated by estimates corresponding to $N_z = 2$ or 3. For $N_k = 8, 9, 10$ the estimates are not as good, although they remain within an order of magnitude. In our opinion this behavior is related to the fact that the POD error (either absolute or relative) is smaller than 10^{-14}, the tolerance for double precision. Thus, rounding errors have a significant contribution in the final result. Nevertheless, even for this case the estimate (of order 10^{-6}) describes well the forward error (which has an order of 10^{-7}).

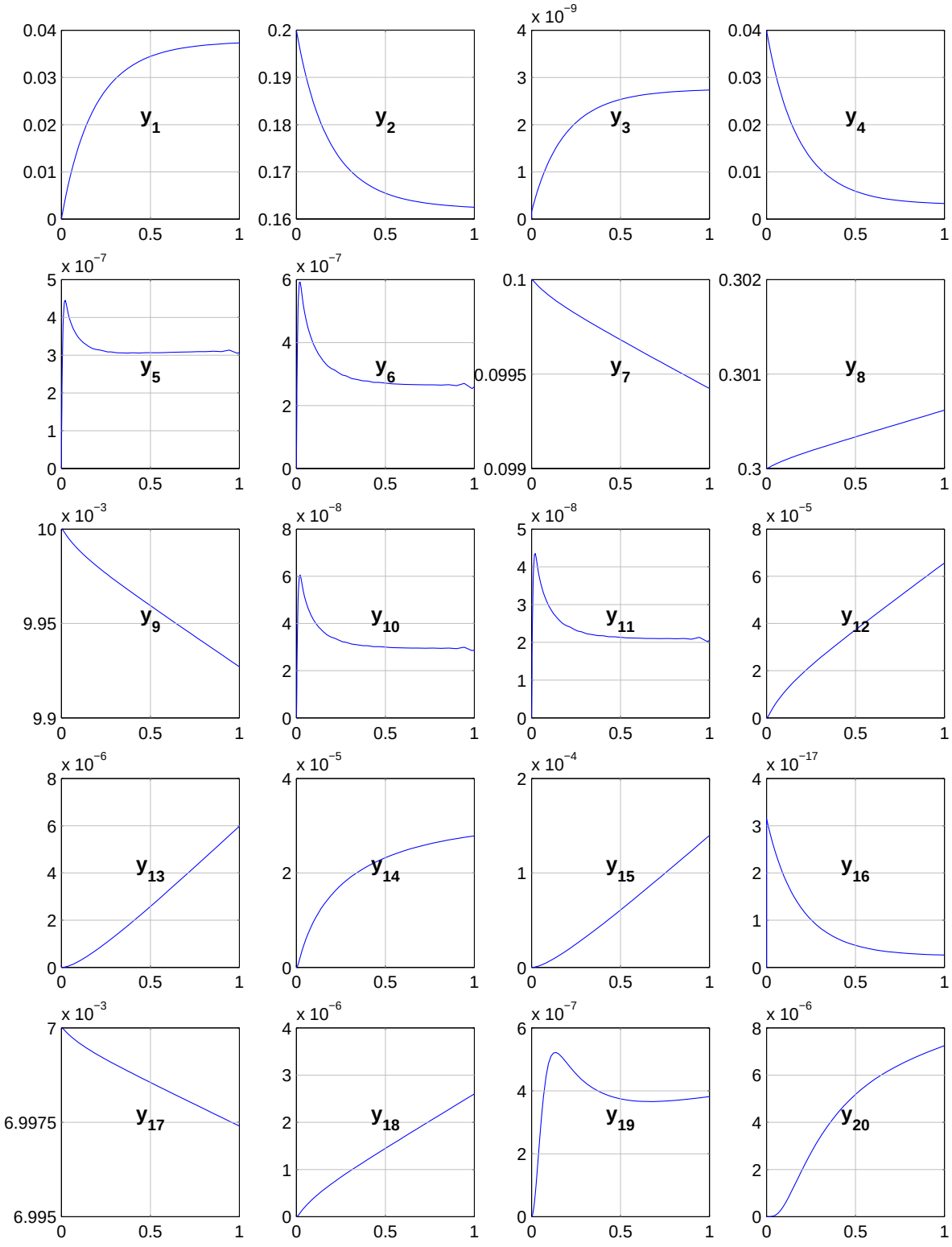

Figure 7: Pollution example. Behavior of the solution over the integration interval.

Table 3: Auxiliary variables and model parameters for the pollution model

Auxiliary variables r_j				
$r_1 = k_1 y_1$	$r_6 = k_6 y_7 y_6$	$r_{11} = k_{11} y_{13}$	$r_{16} = k_{16} y_4$	$r_{21} = k_{21} y_{19}$
$r_2 = k_2 y_2 y_4$	$r_7 = k_7 y_9$	$r_{12} = k_{12} y_{10} y_2$	$r_{17} = k_{17} y_4$	$r_{22} = k_{22} y_{19}$
$r_3 = k_3 y_5 y_2$	$r_8 = k_8 y_9 y_6$	$r_{13} = k_{13} y_{14}$	$r_{18} = k_{18} y_{16}$	$r_{23} = k_{23} y_1 y_4$
$r_4 = k_4 y_7$	$r_9 = k_9 y_{11} y_2$	$r_{14} = k_{14} y_1 y_6$	$r_{19} = k_{19} y_{16}$	$r_{24} = k_{24} y_{19} y_1$
$r_5 = k_5 y_7$	$r_{10} = k_{10} y_{11} y_1$	$r_{15} = k_{15} y_3$	$r_{20} = k_{20} y_{17} y_6$	$r_{25} = k_{25} y_{20}$
Model parameters				
$k_1 = 0.350 \cdot 10^{0}$	$k_6 = .150 \cdot 10^{5}$	$k_{11} = .220 \cdot 10^{-1}$	$k_{16} = .350 \cdot 10^{-3}$	$k_{21} = .210 \cdot 10^{1}$
$k_2 = 0.266 \cdot 10^{2}$	$k_7 = .130 \cdot 10^{-3}$	$k_{12} = .120 \cdot 10^{5}$	$k_{17} = .175 \cdot 10^{-1}$	$k_{22} = .578 \cdot 10^{1}$
$k_3 = .123 \cdot 10^{5}$	$k_8 = .240 \cdot 10^{5}$	$k_{13} = .188 \cdot 10^{1}$	$k_{18} = .100 \cdot 10^{9}$	$k_{23} = .474 \cdot 10^{-1}$
$k_4 = .860 \cdot 10^{-3}$	$k_9 = .165 \cdot 10^{5}$	$k_{14} = .163 \cdot 10^{5}$	$k_{19} = .444 \cdot 10^{12}$	$k_{24} = .178 \cdot 10^{4}$
$k_5 = .820 \cdot 10^{-3}$	$k_{10} = .900 \cdot 10^{4}$	$k_{15} = .480 \cdot 10^{7}$	$k_{20} = .124 \cdot 10^{4}$	$k_{25} = .312 \cdot 10^{1}$

Similar reasoning can be employed for the results obtained for IC and RHS perturbations. Moreover one should take into account the fact that the problem is very stiff, such that the integration tolerances had to be given relatively high values of $rtol = 10^{-4}$ and $atol = 10^{-7}$.

Taking that into account, one can expect a less uniform behavior if the results are in the neighborhood of 10^{-7}. And that is indeed observed for the RHS perturbation. But one should notice that, even for that case, the bounds are within an order of magnitude of the forward error.

An additional explanation is necessary for a better understanding of the RHS perturbation results. Since the 25 problem parameters presented in Table 3 have order of magnitudes ranging from 10^{-3} to 10^{12}, not all parameters were considered in the RHS perturbation (our results were obtained using 3 parameters, namely the fourth, the fifth and the seventh).

6 Conclusions and Future Work

We have presented effective methods for estimating approximation errors due to model reduction and regions of validity of such reduced models. The bounds defining these regions of validity are *a-priori*, in the sense that they do not rely on the solution of the perturbed system. The proposed approach, based on SCE norm estimates combined with adjoint models, allows the definition and construction of so-called "error condition numbers" which can be used to assess the size of errors induced by perturbations (in initial conditions or in the model itself) without having to solve the perturbed system.

The performance of the proposed methods was exemplified on several test problems arising from semi-discretizations of time-dependent PDEs, chemical reaction mechanisms, and plant physiology.

We plan to continue this research by first studying the influence of the data set used in constructing the POD basis on the approximation errors and on the regions of validity of the resulting reduced model. In some cases, using data at equally-spaced time points may be inappropriate (or, if using data from measurments, not available). In the case of stiff systems for example, we think that data from the initial fast transient phase should not be included in the construction of the POD basis. Many dynamical systems of interest exhibit both rapidly varying transients (where the solution changes rapidly over a small time scale) and slowly varying transients (where the solution changes slowly over a large time scale). If the rapidly varying transient is represented by very few snapshots, weighted POD decomposition may be considered. The new basis obtained with weighted snapshots will be able to represent the system behaviour much better compared to the basis functions obtained with the classical POD decomposition technique [21]. The methodology that we have developed in this research can be easily extended to errors for weighted POD-reduced models.

Secondly, we wish to investigate methods for incremental update of the POD basis from simulation data during the forward integration of the original ODE. For large-scale models, it is inefficient (sometimes even untractable) to build and apply an SVD on the data matrix $\mathcal{Y}$.

References

[1] A.C. Antoulas and D.C. Sorensen. Approximation of large-scale dynamical systems: An overview. Technical Report TR0101, Rice University, 2001.

[2] E. Balsa-Canto, A.A. Alonso, and J.R. Banga. A novel, efficient and reliable method for thermal process design and optimization. Part I: theory. Part II: applications. *Journal of Food Processing*, 52(3):227–247, 2002.

[3] H.T. Banks, M.L. Joyner, B. Wincheski, and W.P. Winfree. Real time computational algorithms for eddy-current-based damage detection. *Inverse problems*, 18(3):795–823, 2002.

[4] Y. Cao and L.R. Petzold. A posteriori error estimation and global error control for ordinary differential equations by the adjoint method. *SIAM J. Sci. Comp.*, 2002.

[5] E. Caraballo, M. Saminy, J. Scott, S. Narayan, and J. DeBonis. Application of proper orthogonal decomposition to a supersonic axisymmetric jet. *AIAA Journal*, 41(5):866–877, 2003.

[6] P.G.A. Cizmas and A. Palacios. Proper orthogonal decomposition of turbine rotor-stator interaction. *Journal Of Propulsion And Power*, 19(2):268–281, 2003.

[7] G. H. Golub and C. F. Van Loan. *Matrix computations*. The Johns Hopkins University Press, Baltimore, Md, 1996.

[8] T. Gudmundsson, C.S. Kenney, and A.J. Laub. Small-sample statistical estimates for matrix norms. *SIAM J. Matrix Anal. Appl.*, 16(3):776–792, 1995.

[9] E. Hairer and G. Wanner. *Solving ordinary differntial equations II: Stiff and differential Algebraic problems*. Springer, 1987.

[10] P. Holmes, J.L. Lumley, and G. Berkooz. *Turbulence, coherent structures, dynamical systems and symmetry*. Cambridge University Press, 1998.

[11] C.S. Kenney and A.J. Laub. Small-sample statistical condition estimates for general matrix functions. *SIAM J. Sci. Comp.*, 15(1):36–61, 1994.

[12] H. Kikuchi, Y. Tamura, H. Ueda, and K. Hibi. Dynamic wind pressures acting on a tall building model - proper orthogonal decomposition. *Journal Of Wind Engineering And Industrial Aerodynamics*, 71:631–646, 1997.

[13] M.E. Kowalski and H.M. Jin. Model-order reduction of nonlinear models of electromagnetic phased-array hyperthermia. *IEEE Transactions On Biomedical Engineering*, 50(11):1243–1254, 2003.

[14] K. Kunisch and S. Volkwein. Control of the Burgers equation by a reduced-order approach using proper orthogonal decomposition. *Journal Of Optimization Theory And Applications*, 102(2):345–371, 1999.

[15] K. Kunisch and S. Volkwein. Galerkin proper orthogonal decomposition methods for a general equation in fluid dynamics. *Siam Journal On Numerical Analysis*, 40(2):492–515, 2002.

[16] P.A. LeGresley and J.J. Alonso. Dynamic domain decomposition and error correction for reduced order models. AIAA 2003-0250, 2003.

[17] C. Lopez and E. Garcia-Herandez. Low-dimensional dynamical system model for observed coherent structures in ocean satellite data. *Physica A- Statistical Mechanics and its Applications*, 328(1-2):233–250, 2003.

[18] H.V. Ly and H.T. Tran. Modeling and control of physical processes using proper orthogonal decomposition. *Mathematical and Computer Modelling*, 33(1-3):223–236, 2001.

[19] X. Ma and G.E. Karniadakis. A low-dimensional model for simulating three-dimensional cylinder flow. *Journal of Fluid Mechanics*, 458:181–90, 2002.

[20] M. Meyer and H.G. Matthies. Efficient model reduction in non-linear dynamics using the karhunen-loeve expansion and dual-weighted-residual methods. *Computational Mechanics*, 31(1-2):179–191, 2003.

[21] R. Qiao and N.R. Aluru. Transient analysis of electro-osmotic transport by a reduced-order modelling approach. *International Journal For Numerical Methods In Engineering*, 56(7):1023–1050, 2003.

[22] M. Rathinam and L.R. Petzold. A new look at proper orthogonal decomposition. *SIAM J. Num. An.*, submitted, 2002.

[23] S.S. Ravindran. A reduced-order approach for optimal control of fluids using proper orthogonal decomposition. *International Journal for Numerical Methods in Fluids*, 34(5):425–448, 2000.

[24] J.A. Rule, R.E. Richard, and R.L. Clark. Design of an aeroelastic delta wing model for active flutter control. *Journal Of Guidance Control And Dynamics*, 24(5):918–924, 2001.

[25] B. Shapiro. Creating compact models of complex electronic systems: An overview and suggested use of existing model reduction and experimental system identification tools. *IEEE Transactions On Components And Packaging Technologies*, 26(1):165–172, 2003.

[26] Y. Shin and T. Sakurai. Power distribution-analysis of vlsi interconnects using model order reduction. *IEEE Transactions On Computer-Aided Design Of Integrated Circuits And Systems*, 21(6):739–745, 2002.

[27] S. Utku, J.L.M. Clemente, and M. Salama. Errors in reduction methods. *Computers and Structures*, 21(6):1153–1157, 1985.

[28] J.G. Verwer. Gauss-Seidel iteration for stiff ODEs from chemical kinetics. *SIAM J. Sci. Comput.*, 15(5):1243–1259, 1994.

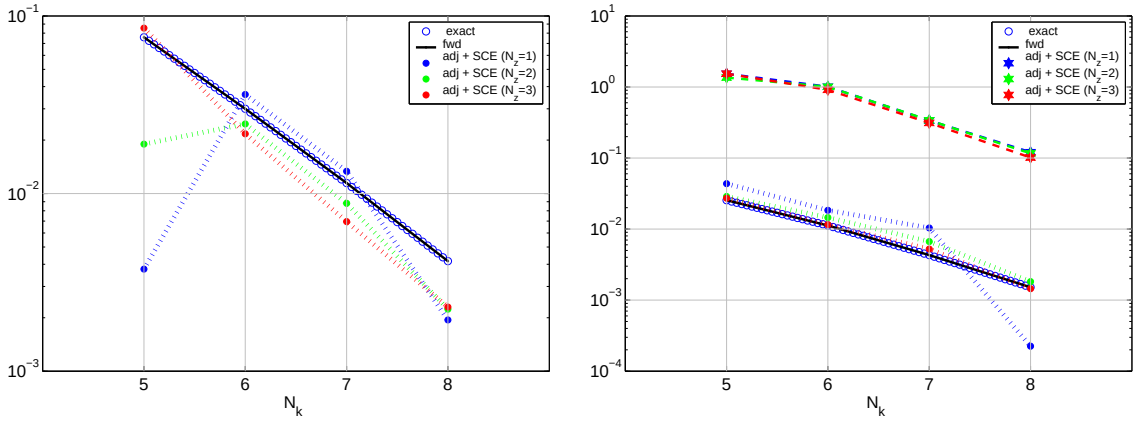

(a) Total error

(b) Subspace integration error

Figure 8: 1D advection-diffusion example. POD approximation error.

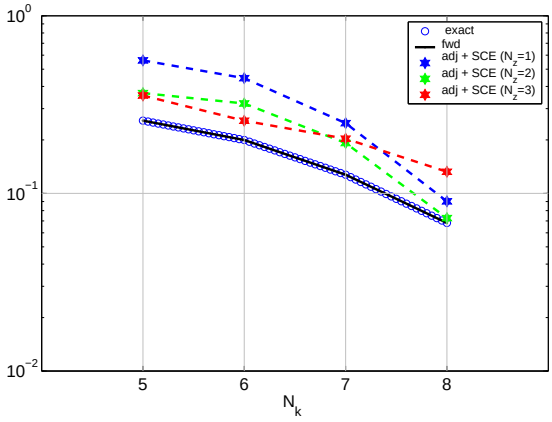

(a) Approximation error E^1 as function of the subspace dimension ($\delta y_0 = 1.0\%$)

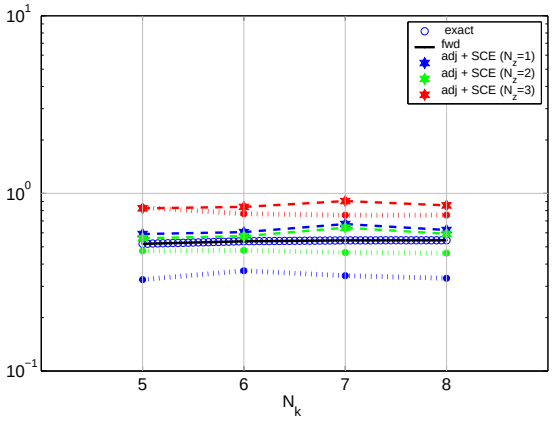

(b) Cumulative error E^2 as function of the subspace dimension ($\delta y_0 = 1.0\%$)

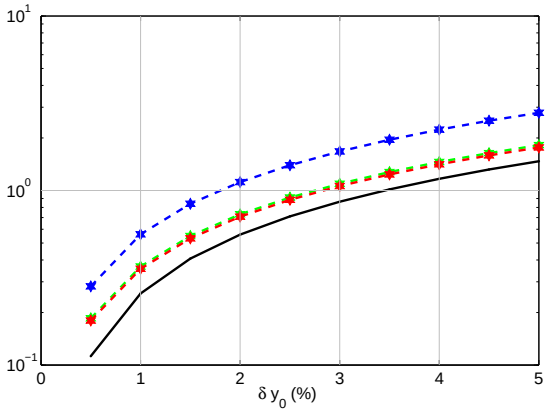

(c) Approximation error E^1 as function of the IC perturbation ($N_k = 5$)

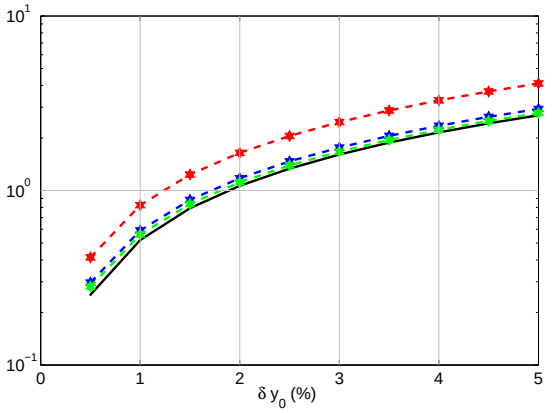

(d) Cumulative error E^2 as function of the IC perturbation ($N_k = 5$)

Figure 9: 1D advection-diffusion example. IC perturbation.

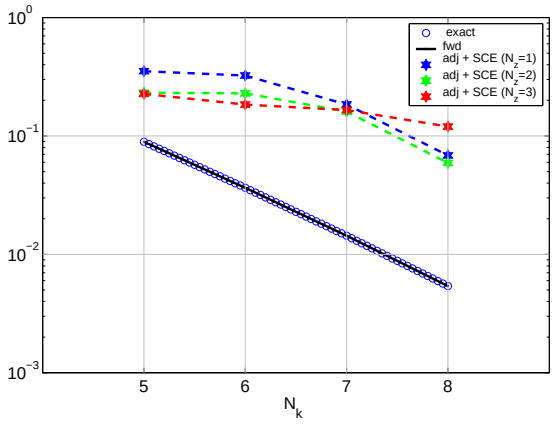

(a) Approximation error E^1 as function of the subspace dimension ($\delta p = 1.0\%$)

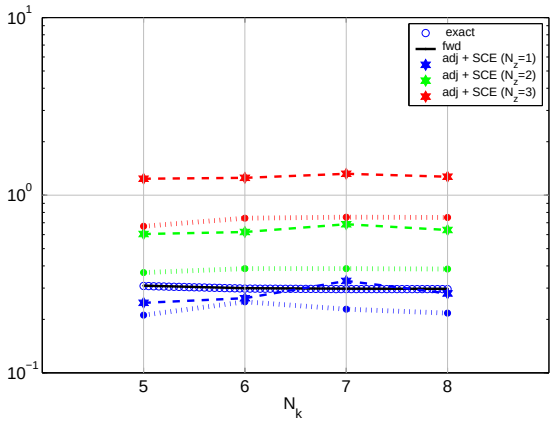

(b) Cumulative error E^2 as function of the subspace dimension ($\delta p = 1.0\%$)

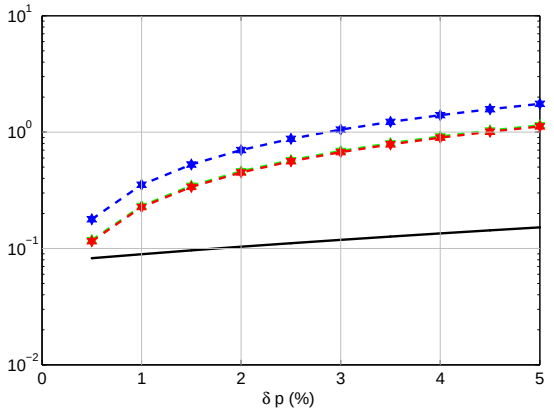

(c) Approximation error E^1 as function of the RHS perturbation ($N_k = 5$)

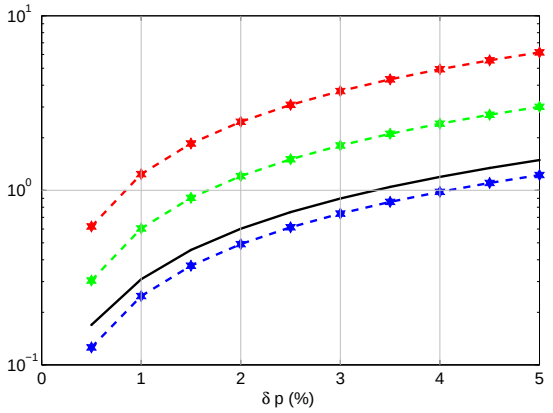

(d) Cumulative error E^2 as function of the RHS perturbation ($N_k = 5$)

Figure 10: 1D advection-diffusion example. RHS perturbation.

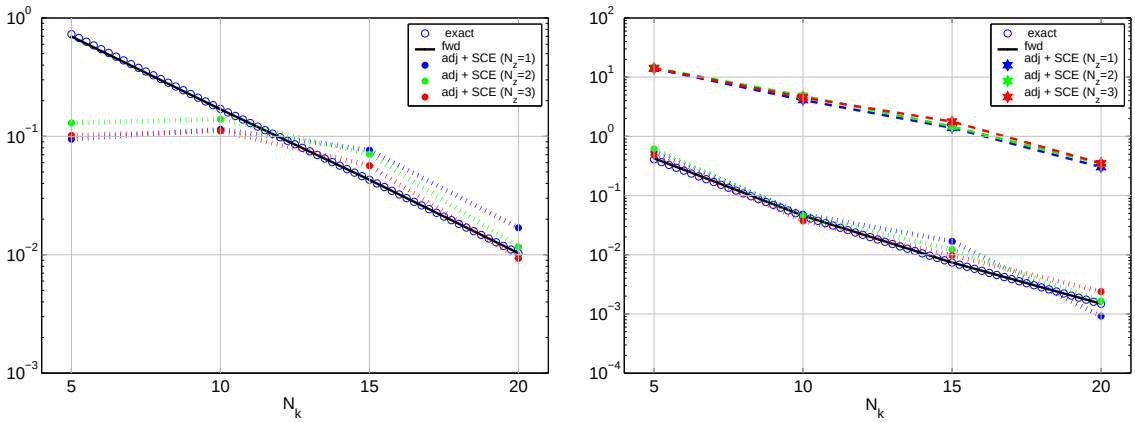

(a) Total error

(b) Subspace integration error

Figure 11: Burger's equation example. POD approximation error.

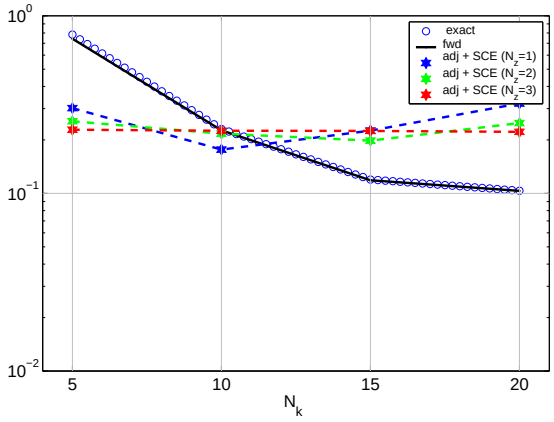

(a) Approximation error E^1 as function of the subspace dimension ($\delta y_0 = 1.0\%$)

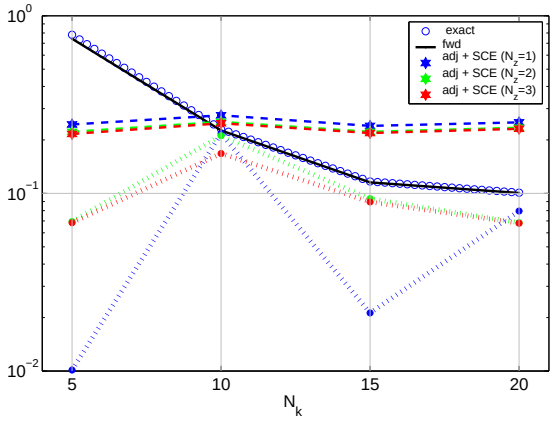

(b) Cumulative error E^2 as function of the subspace dimension ($\delta y_0 = 1.0\%$)

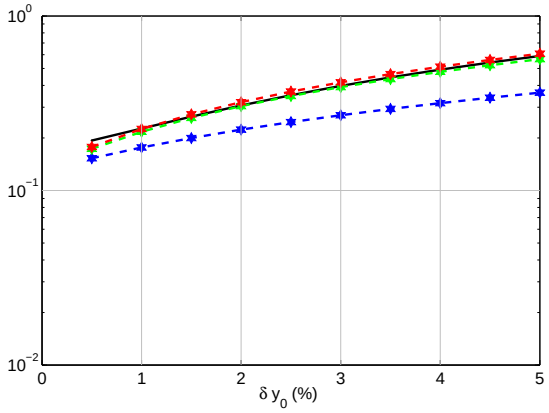

(c) Approximation error E^1 as function of the IC perturbation ($N_k = 10$)

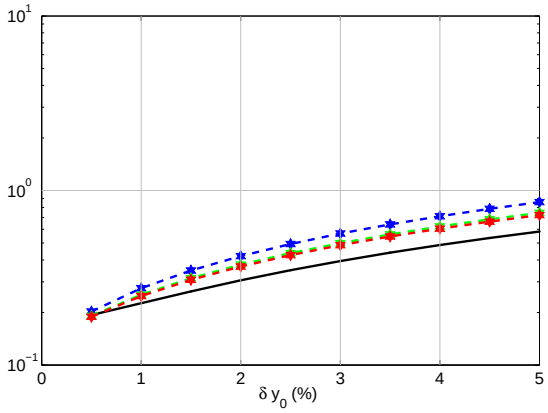

(d) Cumulative error E^2 as function of the IC perturbation ($N_k = 10$)

Figure 12: Burger's equation example. IC perturbation.

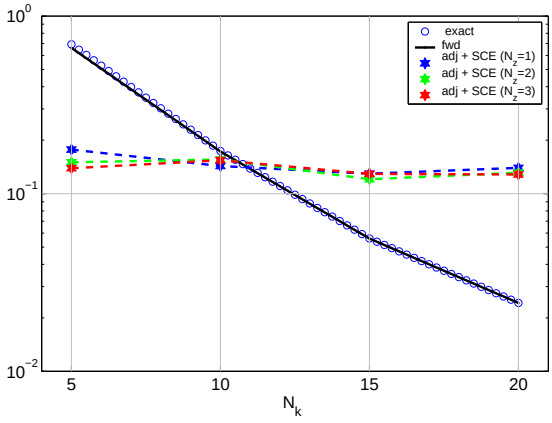

(a) Approximation error E^1 as function of the subspace dimension ($\delta p = 5.0\%$)

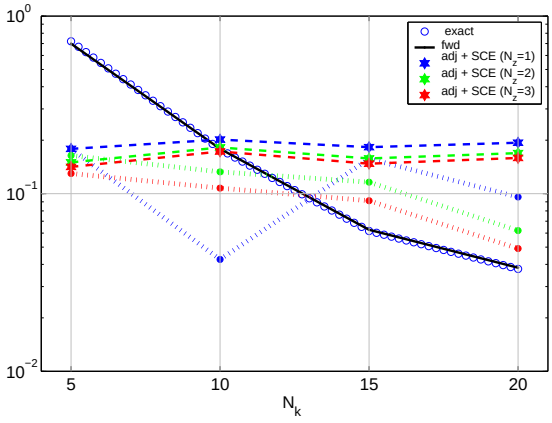

(b) Cumulative error E^2 as function of the subspace dimension ($\delta p = 5.0\%$)

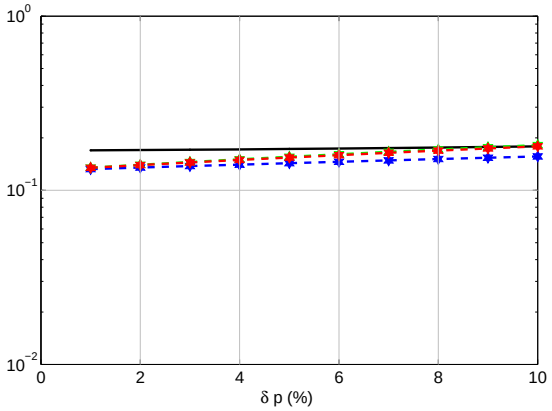

(c) Approximation error E^1 as function of the RHS perturbation ($N_k = 10$)

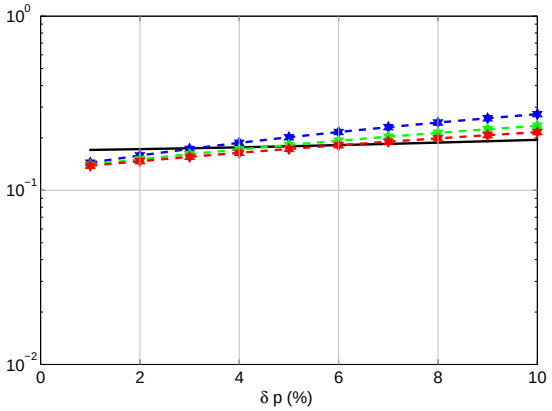

(d) Cumulative error E^2 as function of the RHS perturbation ($N_k = 10$)

Figure 13: Burger's equation example. RHS perturbation.

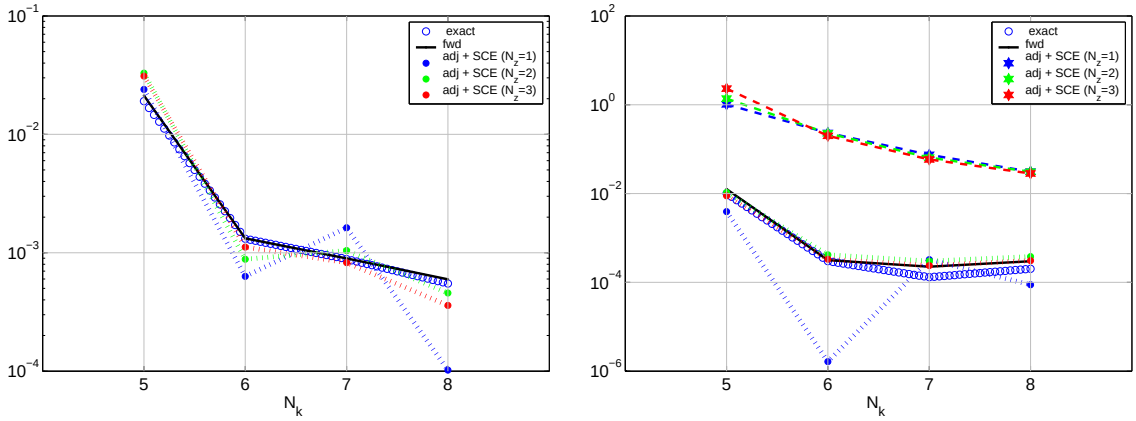

(a) Total error

(b) Subspace integration error

Figure 14: Brusselator example. POD approximation error.

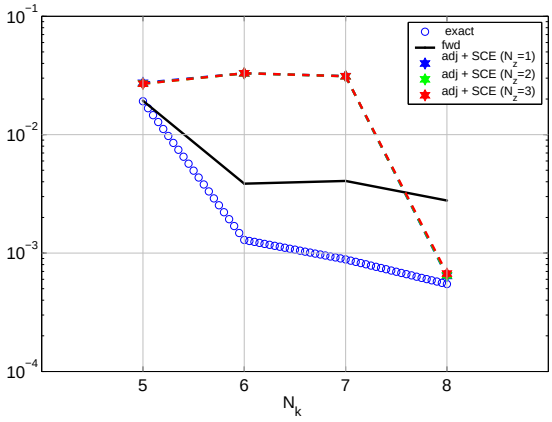

(a) Approximation error E^1 as function of the subspace dimension ($\delta y_0 = 0.5\%$)

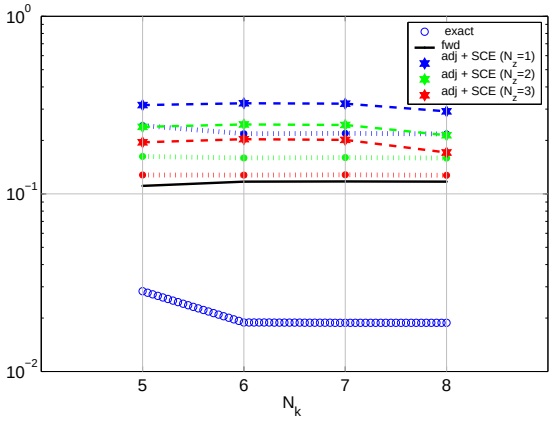

(b) Cumulative error E^2 as function of the subspace dimension ($\delta y_0 = 0.5\%$)

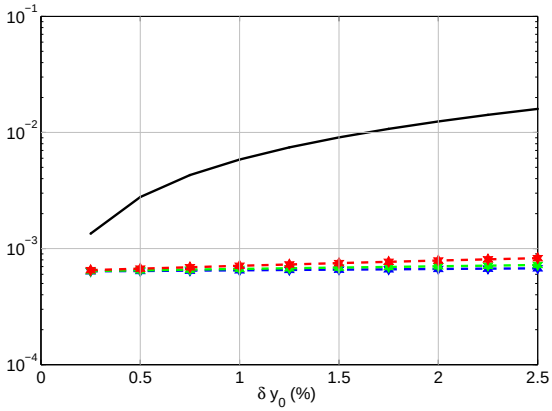

(c) Approximation error E^1 as function of the IC perturbation ($N_k = 8$)

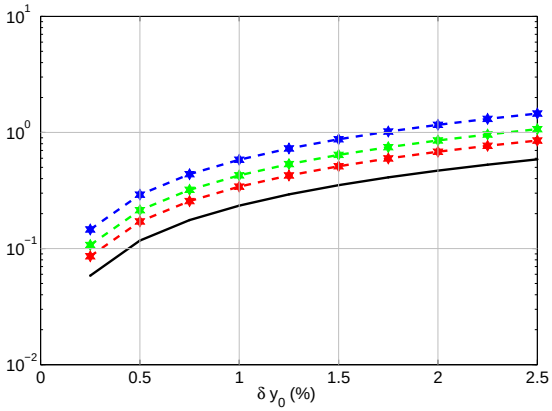

(d) Cumulative error E^2 as function of the IC perturbation ($N_k = 8$)

Figure 15: Brusselator example. IC perturbation.

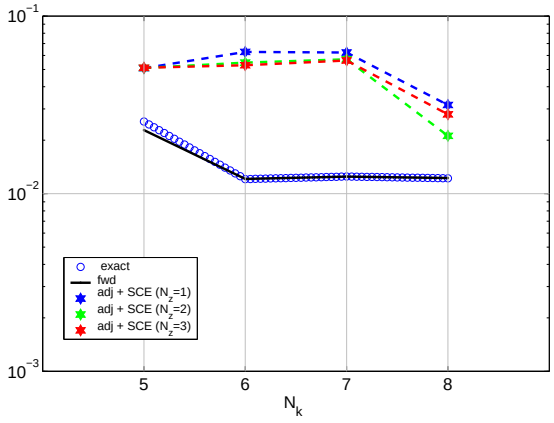

(a) Approximation error E^1 as function of the subspace dimension ($\delta p = 0.1\%$)

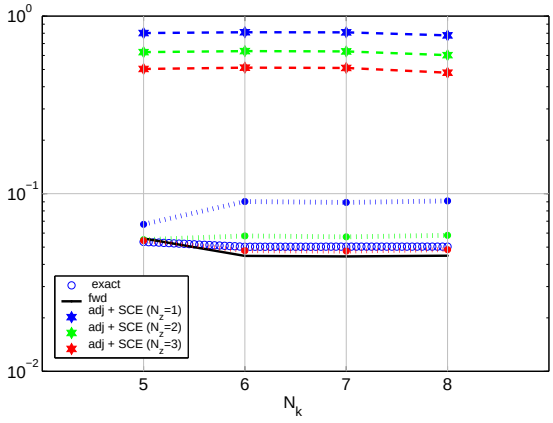

(b) Cumulative error E^2 as function of the subspace dimension ($\delta p = 0.1\%$)

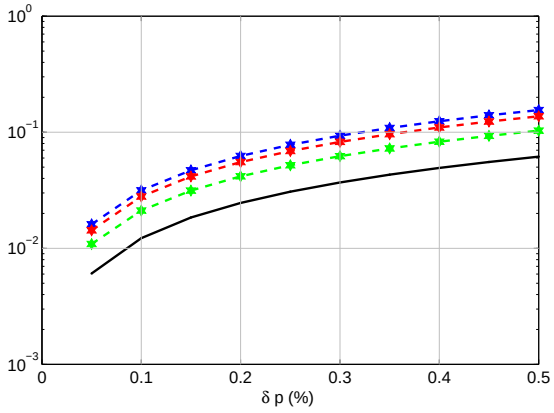

(c) Approximation error E^1 as function of the RHS perturbation ($N_k = 8$)

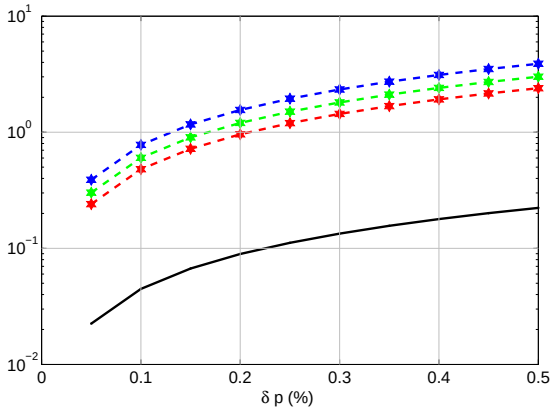

(d) Cumulative error E^2 as function of the RHS perturbation ($N_k = 8$)

Figure 16: Brusselator example. RHS perturbation.

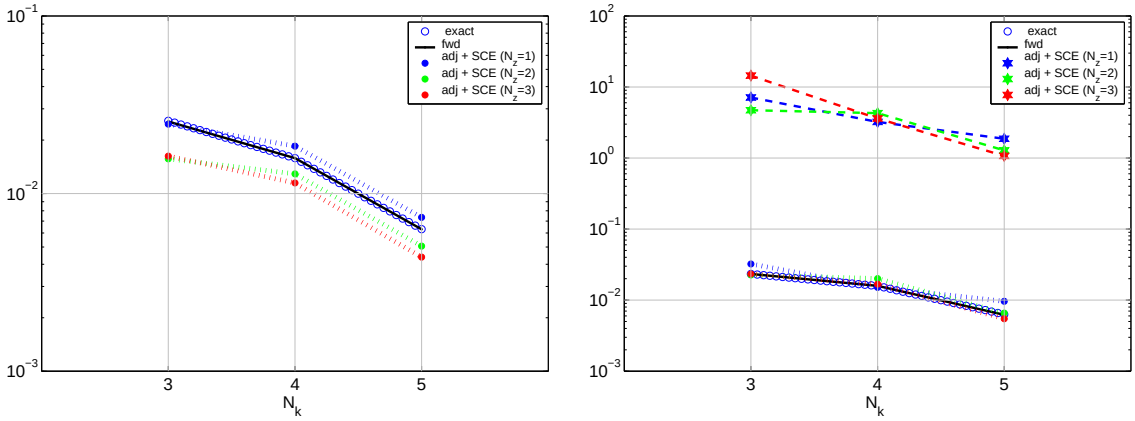

(a) Total error

(b) Subspace integration error

Figure 17: HIRES example. POD approximation error.

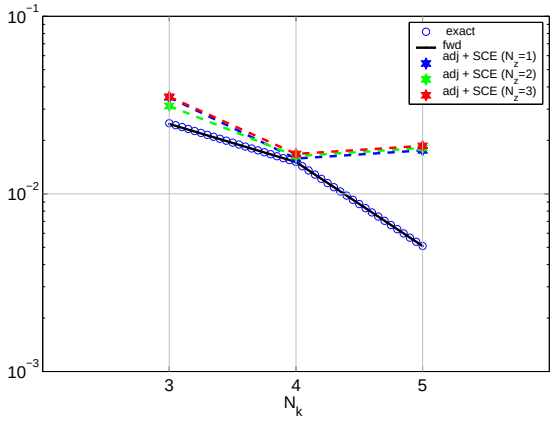

(a) Approximation error E^1 as function of the subspace dimension ($\delta y_0 = 0.1\%$)

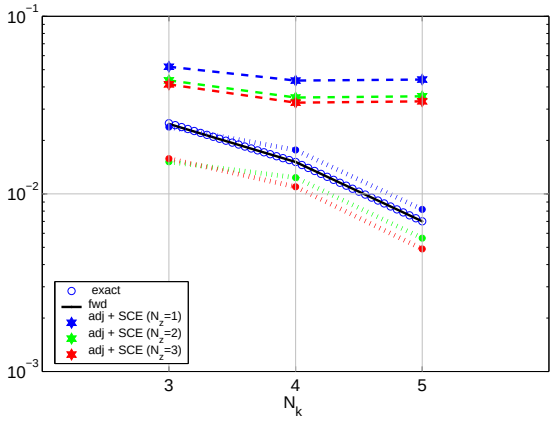

(b) Cumulative error E^2 as function of the subspace dimension ($\delta y_0 = 0.1\%$)

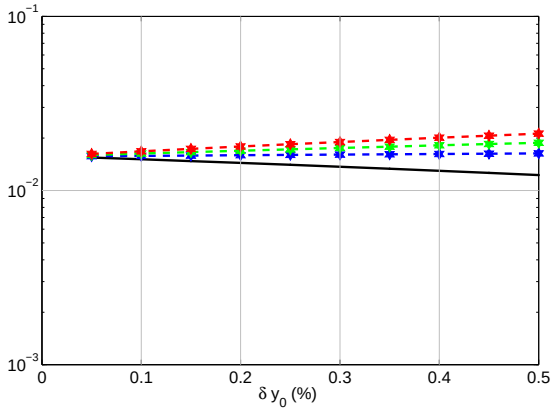

(c) Approximation error E^1 as function of the IC perturbation ($N_k = 4$)

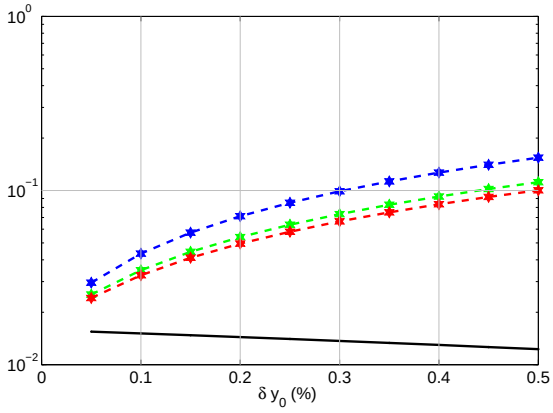

(d) Cumulative error E^2 as function of the IC perturbation ($N_k = 4$)

Figure 18: HIRES example. IC perturbation.

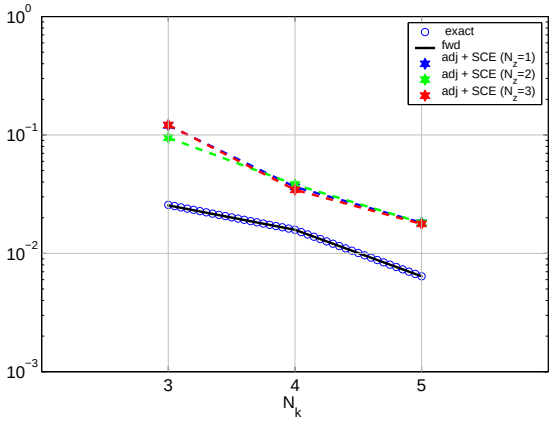

(a) Approximation error E^1 as function of the subspace dimension ($\delta p = 0.1\%$)

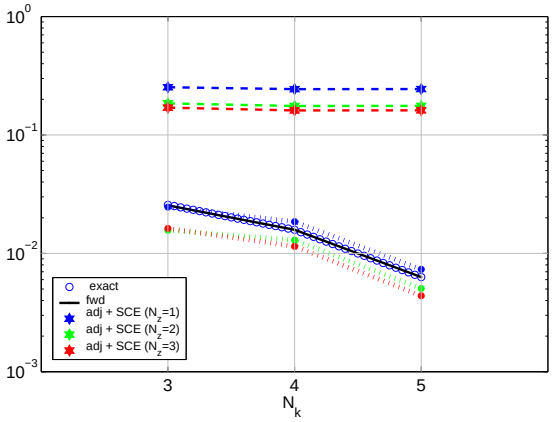

(b) Cumulative error E^2 as function of the subspace dimension ($\delta p = 0.1\%$)

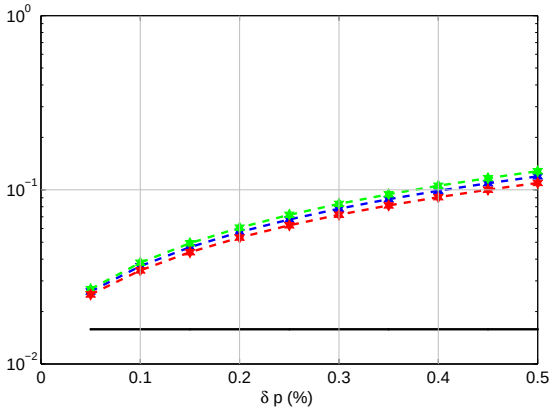

(c) Approximation error E^1 as function of the RHS perturbation ($N_k = 4$)

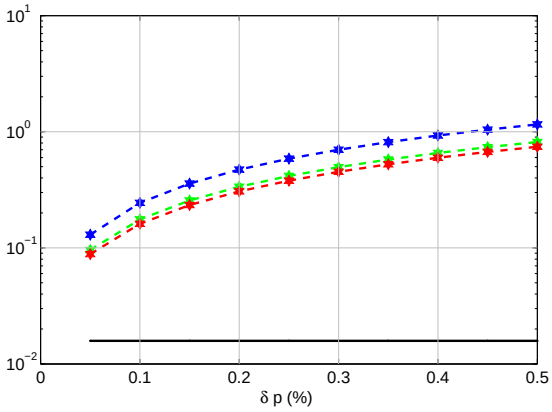

(d) Cumulative error E^2 as function of the RHS perturbation ($N_k = 4$)

Figure 19: HIRES example. RHS perturbation (perturbed parameters were $[k_3, k_4, k_5, k_6]$).

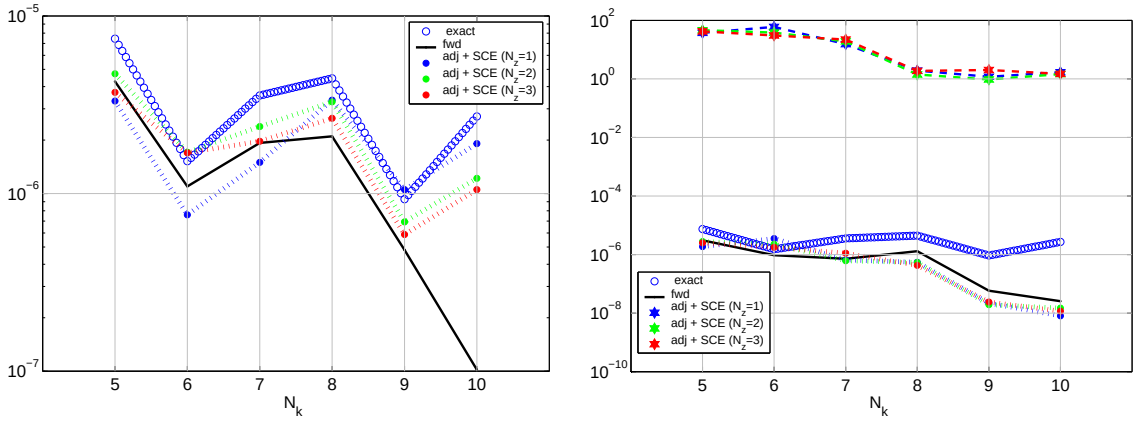

(a) Total error

(b) Subspace integration error

Figure 20: Pollution example. POD approximation error.

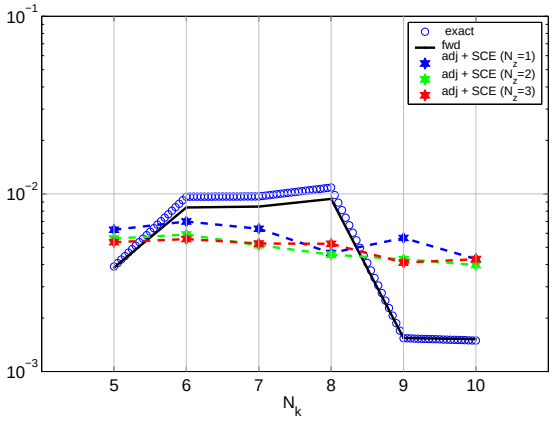

(a) Approximation error E^1 as function of the subspace dimension ($\delta y_0 = 0.3\%$)

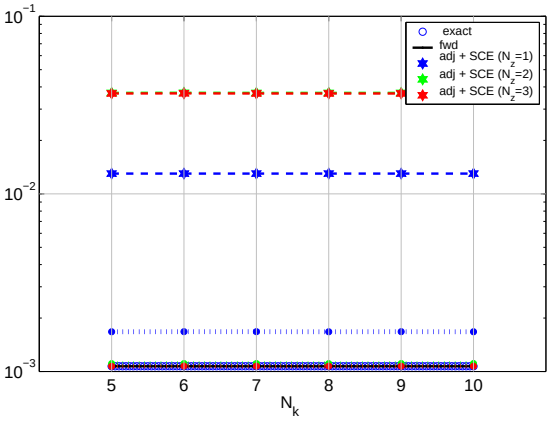

(b) Cumulative error E^2 as function of the subspace dimension ($\delta y_0 = 0.3\%$)

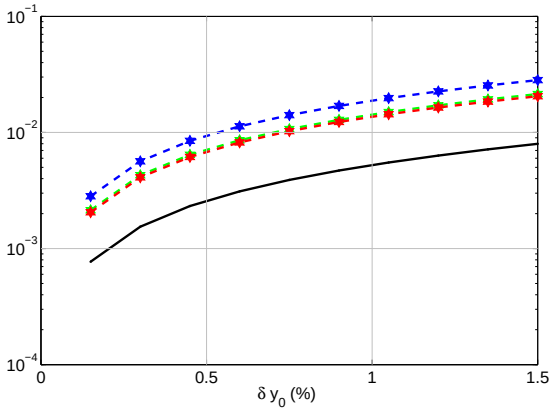

(c) Approximation error E^1 as function of the IC perturbation ($N_k = 5$)

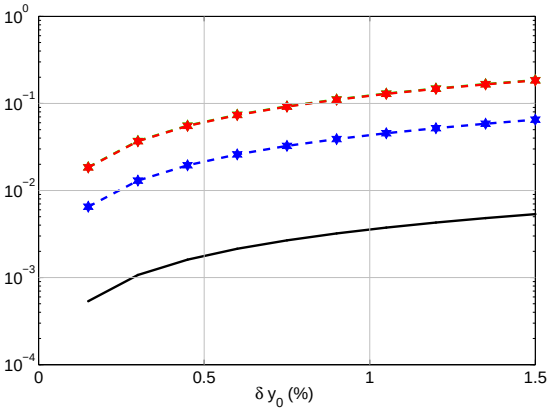

(d) Cumulative error E^2 as function of the IC perturbation ($N_k = 5$)

Figure 21: Pollution example. IC perturbation.

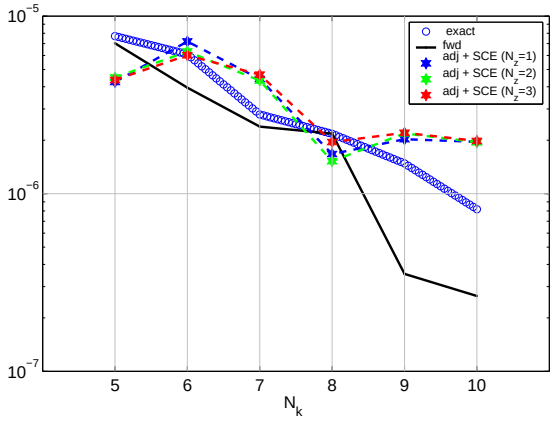

(a) Approximation error E^1 as function of the subspace dimension ($\delta p = 1.0\%$)

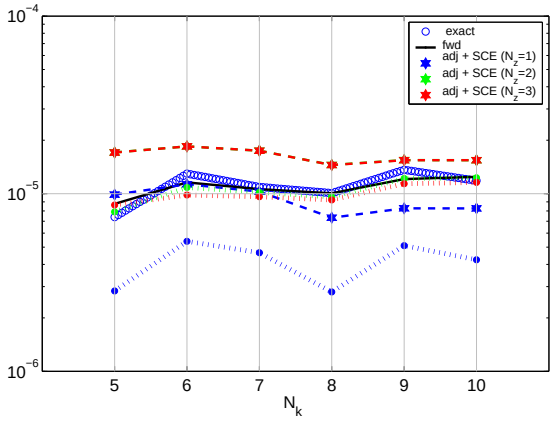

(b) Cumulative error E^2 as function of the subspace dimension ($\delta p = 1.0\%$)

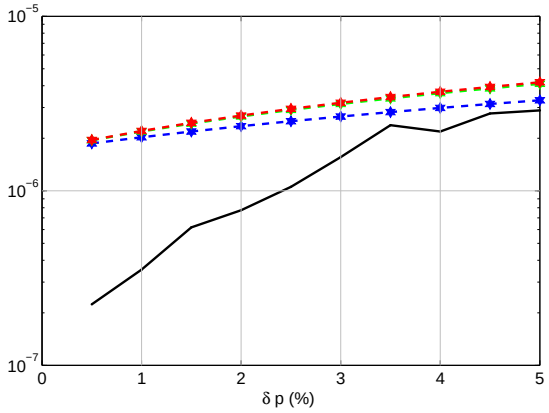

(c) Approximation error E^1 as function of the RHS perturbation ($N_k = 5$)

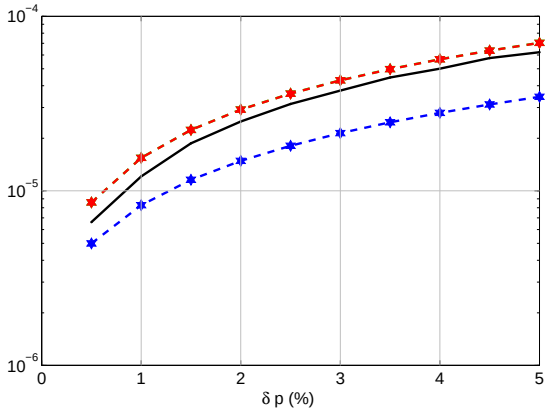

(d) Cumulative error E^2 as function of the RHS perturbation ($N_k = 5$)

Figure 22: Pollution example. RHS perturbation (perturbed parameters were $[k_4, k_5, k_7]$).

University of California
Lawrence Livermore National Laboratory
Technical Information Department
Livermore, CA 94551